FINAL REPORT: BASIC RESEARCH AT THE UNIVERSITY OF WASHINGTON TO COUNTER IMPROVISED EXPLOSIVE DEVICES

by

Jeffrey A. Simmen, Eric I. Thorsos, William E. Asher, Antao Chen, Lawrence A. Crum, William T. Elam, Maya Gupta, Yasuo Kuga, Caren Marzban, and Dale P. Winebrenner

University of Washington

Sponsor: Office of Naval Research
Grant N00014-05-1-0843

Approved for Public release; distribution unlimited.

Final Report for ONR CODE 30 CIED 6.1 Basic Research Effort

1. **"Nonlinear Optical Methods for Remotely Identifying Trace Amounts of Explosives"**
2. **Prime Offeror:** Applied Physics Laboratory, University of Washington
3. **Subcontractors:** none
4. **Period of Performance:** 08/01/2005 – 12/31/2009
5. **Submitted by:** William E. Asher, asher@apl.washington.edu, 206-543-5942
6. **Business Contact:** Monty Bolstad, monty@apl.washington.edu, 206-543-9826

7. **Background/Scope of Effort**

Stand-off detection of explosive devices using some form of remote spectroscopic analysis would be of great benefit. It is possible that the nonlinear spectroscopic technique of sum frequency generation (SFG) could be used as a remote-sensing probe for detecting trace levels of explosive materials on surfaces. The goal of this research is to understand the relationship between the surface concentration of high explosives and the net nonlinear optical response for homogeneous and heterogeneous substrates. This information will be used to establish the theoretical detection limits these optical responses imply towards the remote detection of trace levels of explosives using SFG.

8. **Summary/Abstract**

Stand-off detection of trace levels of explosives would be of great benefit in identifying the location of hidden explosive devices and locations where these munitions are assembled. This research under the ONR Counter-IED (ONR-CIED) program has been investigating the use of the nonlinear optical technique vibrational sum frequency generation spectroscopy (VSFGS) for detecting trace levels of explosives on surfaces. So far, our work has demonstrated that VSFGS can detect the explosives 2,4,6-trinitrophenol (picric acid), 2,4,6-trinitrotoluene (TNT) and 1,3,5-trinitro-1,3,5-triazacyclohexane (RDX) at surface concentrations as low as 300 ng cm^{-2}. Because these surface concentrations are typical of what might be found on surfaces containing adventitious contamination of explosives [*Stott et al.*, 1994], these laboratory results indicate that VSFGS could be used as a remote-sensing probe for detecting trace levels of explosives.

9. **Technical Contents and Accomplishments**

Summary of Prior Results: Experiments conducted under our ONR CIED research project have demonstrated the following results:

1. Explosives containing multiple nitro ($-NO_2$) groups have very large nonlinear optical cross sections and VSFGS can easily detect these explosives on surfaces at concentrations as low as 300 ng cm^{-2} (see Figure 1).
2. VSFGS can detect nitro group-containing explosives on rough metal surfaces that might be encountered in the field, including galvanized steel, T6061 aluminum alloy, and inorganic mineral dust (see Figure 2).
3. Detection times for explosives using VSFGS would be rapid, possibly as low as a few hundred milliseconds, because full spectral resolution of VSFGS signal is not required.

4. The infrared (IR) wavelength of the molecular vibration that is used for VSFGS of explosives occurs in a spectral region where IR atmospheric propagation permits maximum theoretical stand-off distances of several hundred meters (see Figure 3).
5. Decomposition of an explosive under environmental conditions leads to a measurable change in the VSFGS response of that explosive (see Figure 4).
6. Compounds containing -NO_2 groups might be produced in photochemical smog that could interfere with the detection of explosives under field conditions (see Figure 5).

These results are discussed in detail in the following section.

Detailed Discussion: The threat of improvised explosive devices (IEDs) to human life is grave, and countering this threat is a high priority for force protection during military operations. Remote, stand-off detection of in-place IEDs would be a significant step forward in mitigating the threat posed by these weapons. Because of the low vapor pressures of most high explosives (HEs) [*CREPSEDT*, 2004], it is extremely difficult to detect their presence in the gas phase using methods that might be adapted as stand-off systems. For example, although cavity ring-down laser spectroscopy (CRLS) has the sensitivity to detect explosives in the gas phase [*Fidric et al.*, 2003], it is not amenable to stand-off application [*CREPSEDT*, 2004]. However, explosives are known to adsorb on surfaces due to their high electronegativity and low vapor pressure [*CREPSEDT*, 2004], and methods relying on detecting their presence on surfaces show promise for remote-sensing applications.

Optical sum-frequency generation (SFG) has long been used for studying surface chemistry [*Lambert et al.*, 2005; *Shen*, 2000]. SFG is a second-order two-photon-mixing process, where the nonlinear interaction between the electromagnetic dipole of a molecule and two incident photons with frequencies ω_1 and ω_2, respectively, leads to the generation of a photon with frequency equal to $\omega_S = \omega_1 + \omega_2$. As a concrete example of this process, when photons having wavelengths of 1064 nm and 532 nm illuminate the surface of urea crystals, photons with wavelengths of 355 nm (in the ultraviolet spectral region) can be detected.

Theoretical considerations show that to a first approximation, sum-frequency generation (SFG) emissions occur only from the surface of an isotropic material such as metals, liquids, or glasses [*Shen*, 1984; 1999]. Furthermore, it has been shown that SFG has the capability to detect sub-monomolecular coverage of molecules adsorbed on surfaces [*Shen*, 2000]. Given the likelihood that HEs will be present on surfaces at low concentrations, surface selectivity and high sensitivity to surface chemistry are key advantages of VSFGS in detecting HEs.

The number of photons generated at ω_S is a function of the incident light intensity, the nonlinear optical properties of the material, and the presence of any resonances between vibrational molecular energy transitions and the energy of the incident or outgoing photons [*Shen*, 2000]. This dependence is expressed in terms of the total second order nonlinear polarization of the surface $P^{(2)}$. It can be shown that the SFG intensity is proportional to the three orthogonal components of $P^{(2)}$ at frequency ω_S, which are given by [*Lambert et al.*, 2005]

$$P_i^{(2)}(\omega_S) = \varepsilon_0 \sum_j \sum_k \chi_{ijk}^{(2)} E_j(\omega_1) E_k(\omega_2) \quad (1)$$

where ε_0 is the vacuum permittivity, $\chi_{ijk}^{(2)}$ is the *i*'th, *j*'th, *k*'th component of the second order surface nonlinear response tensor of the system, $\chi^{(2)}$, and $E_j(\omega_1)$ and $E_k(\omega_2)$ are the *j*'th and *k*'th components, respectively, of the electromagnetic fields of the incident laser beams at frequencies ω_1 and ω_2, respectively.

In order to calculate signal intensities, the macroscopic nonlinear surface susceptibility, $\chi^{(2)}$, must be related to the nonlinear polarizability of the individual molecules adsorbed on the surface, $\beta^{(2)}$, and to the polarizability of the surface itself. In general the elements of $\chi^{(2)}$ will not be identical to the elements of $\beta^{(2)}$, and molecular symmetry and orientation will be important in determining the overall nonlinear optical response of the system [*Lambert et al.*, 2005]. In relation to VSFGS, it is the behavior of $\beta^{(2)}$ when the frequency of one of the incoming laser beams is near the frequency of a vibrational band that is most important. Near a molecular vibrational mode with frequency ω_v, when $\omega_1 >> \omega_v$ it can be shown that $\beta^{(2)}$ can be estimated from the Raman and vibrational transition moments using [*Hunt et al.*, 1987]

$$\beta_{\alpha\beta\gamma} = \frac{1}{2\hbar} \frac{M_{\alpha\beta} A_\gamma}{(\omega_v - \omega_2 - i\Gamma)} \quad (2)$$

where $M_{\alpha\beta}$ is the Raman transition moment, A_γ is the IR transition moment, ω_2 is the frequency of the incoming IR beam, and Γ^{-1} is the relaxation time of the excited state. Eq. (2) shows that a general selection rule of VSFS is that for a particular vibrational transition to be resonant for SFG, it must be active as both a Raman and an IR band. However, Eq. (2) also shows that the SFG signal arising from the surface polarization can increase by orders of magnitude when $\omega_2 = \omega_v$. Because vibrational transitions of organic molecules occur mainly at IR wavelengths, for VSFGS the wavelength of one incoming laser beam must be tunable in the IR region. Because the VSFGS response of explosives was unknown, the research conducted for our project focused in part on determining whether commonly encountered explosives have nonlinear optical responses that are high enough that would allow VSFGS to be used to detect trace levels of HEs, whether there are vibrational bands of explosives that can be used for remote sensing applications, and whether the interaction between the SFG response of the surface itself will degrade the SFG response of HEs adsorbed on the surface.

Many explosives (*e.g.*, TNT, RDX, HMX) contain multiple nitro ($-NO_2$) groups, and the vibrational modes of $-NO_2$ are known to have large $\chi^{(2)}$ [*Heinz et al.*, 1983]. In particular, the symmetric stretch of $-NO_2$ occurs in the mid-wave IR region at a wavenumber of approximately 1325 cm^{-1}, corresponding to a wavelength of 7.55 μm. Figure 1 shows a plot of the SFG signal intensity in arbitrary units, I_{SFG}, of the symmetric stretch of $-NO_2$ of three explosives: picric acid, RDX, and TNT measured on a fused silica substrate plotted versus surface concentration. Also shown on Figure 1 is I_{SFG} for *p*-nitroaniline (PNA). The data show that I_{SFG} is above the detection threshold at concentrations of a few hundred nanograms per square centimeter in the case of TNT and significantly lower concentrations for RDX and picric acid. Furthermore, I_{SFG} of the three explosives, while being less than that of PNA as a function of concentration, are

still significant in comparison. This is important because PNA has an extremely high $\chi^{(2)}$ [*Zyss*, 1993], so the data in Figure 1 show that $\chi^{(2)}$ for explosives, while not being as high as PNA, are still quite large (in comparison, I_{SFG} for 2-propanol was 1.23 at a surface concentration of 1000 μg cm^{-2}). Figure 1 demonstrates that explosives containing nitro groups have large $\chi^{(2)}$ and can be detected at low surface concentrations using VSFGS.

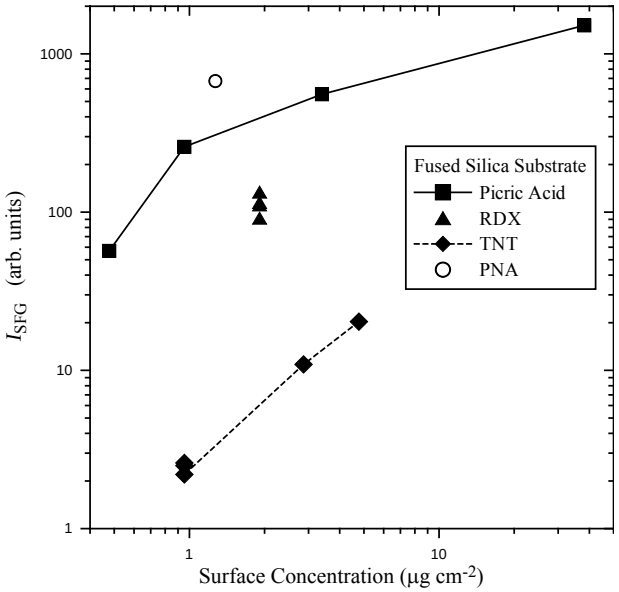

Figure 1. Vibrational sum-frequency generation signal intensities, I_{SFG}, plotted as a function of surface concentration for the explosives picric acid, RDX, and TNT on a fused silica substrate measured by *Asher and Spott* [2008]. I_{SFG} = 1 represents the lowest surface concentration that would be reliably detected above the background value.

The nonlinear susceptibility of both the surface and the adsorbed molecules on the surface play a role in determining I_{SFG} [*Lambert et al.*, 2005]. Because of the interaction of the adsorbate and substrate, successful application of SFG as a molecular probe requires knowledge of the nonlinear optical response of both the target compound and potential substrates. Therefore, the second objective for our work has been to understand the effect of substrate on I_{SFG} for HEs. Figure 2 shows VSFGS spectra for the symmetric stretch of RDX and TNT on fused silica, unpolished T6061 aluminum alloy, unpolished galvanized steel, and a reference standard dust composed of silicon dioxide (70%), aluminum oxide (20%), ferric oxide (7%), and calcium oxide (3%). Comparison of the spectra between the different surfaces for each explosive shows that there is little change in the wavenumber of the maximum in I_{SFG} for the various substrates. Because the maximum is relatively insensitive to substrate, full spectral resolution of SFG signals will not be required, and measuring I_{SFG} at a single wavelength would be sufficient for detection. This greatly increases the measurement speed. Therefore, demonstrating that the SFG response of HEs is relatively insensitive to substrate is important because maximizing measurement speed is a key requirement for stand-off detection of HEs. Figure 2 also demonstrates that SFG signals can be observed from surfaces that produce both specular (fused silica) and diffuse (the metals and mineral dust) reflections. This is

also an important finding for field applications since most surfaces encountered will produce diffuse reflections.

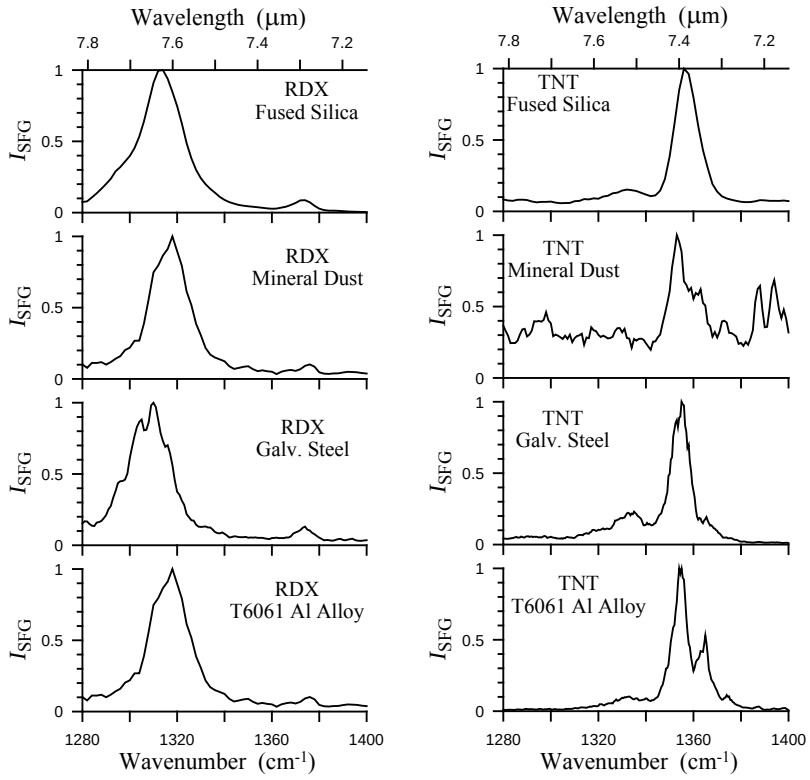

Figure 2. Spectra of thin films of the explosives RDX (left) and TNT (right) on fused silica, mineral dust (see text on page 6 for composition), galvanized steel, and T6061 aluminum plate. The VSFGS signal intensity, ISFG, has been normalized to unity in each spectrum. The surface concentration of explosive for each spectrum was approximately 1 μg cm^{-2}.

The third key finding from our research program was the identification of the symmetric $-NO_2$ stretch as the candidate for VSFGS identification of explosives. Atmospheric propagation of IR light is an issue, and the symmetric $-NO_2$ stretch is found at a wavelength of 7.5 μm. Figure 3 shows that atmospheric propagation distances for IR radiation around this wavelength can be up to several hundred meters with only a 30% loss in total intensity. This implies that in principle it is possible to transmit enough optical power to targets at stand-off distances to generate a return SFG signal (keeping in mind that the returning signal will be at visible wavelengths and not subject to further loss by absorption in the IR).

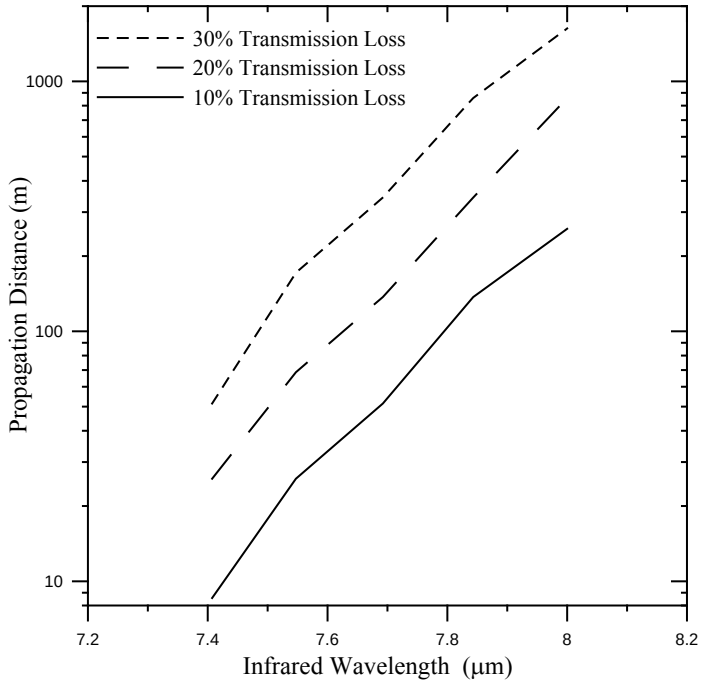

Figure 3. Atmospheric propagation distances for IR light for transmission losses at the 10%, 20%, and 30% level (i.e., the distance at which the IR intensity would be 90%, 80%, and 70%, respectively, of its initial intensity) as a function of wavelength. Atmospheric pressure is 1 atm, air temperature is 27 C, and the relative humidity is 80%.

It was also demonstrated that the VSFGS spectra of explosives changes as degradation occurs. Figure 4 shows spectra of fresh TNT adsorbed on fused silica and TNT that has been exposed to the atmosphere and room lighting for approximately 30 days. Not only is there an overall decrease in the VSFGS response of the aged TNT compared to the fresh material, the peak has shifted to longer wavelengths. This result shows that the aging characteristics of each explosive must be known in order to discriminate the VSFGS signature from fresh explosives from the signal from degraded material.

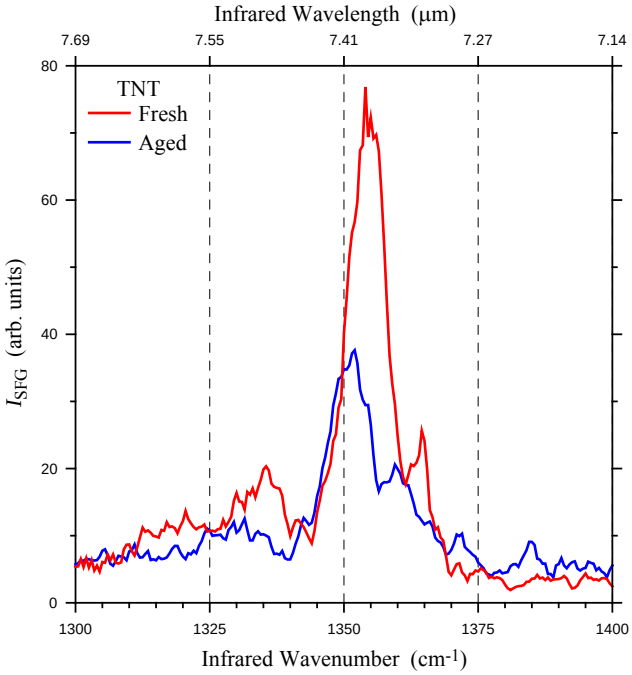

Figure 4. Spectra of fresh TNT and TNT that has been exposed to the atmosphere and fluorescent lights for approximately 30 days. The nominal surface concentration was 2 μg cm^{-2} for both the fresh and aged samples.

Finally, it is known that photochemical smog in an urban environment contains a variety of compounds containing –NO_2 groups [*Griffin et al.*, 2003]. Because the SFG resonances of these pollutants are unknown, it is possible that they could interfere with the detection of explosives. As an initial step in understanding the role of environmental interferences, a photochemical smog model was run to determine both if compounds containing –NO_2 groups would form at concentrations high enough to interfere with VSFGS and also if these compounds would have low enough volatilities to condense on surfaces. Figure 5 shows a time series of the ratio of the mass of a particular smog component found in the particulate phase to the mass found in the gas phase. A value of this ratio greater than one indicates that the compound would be found mainly on particles or other solid surfaces. The results from this effort show that it is possible that low-volatility smog components might condense on surfaces and mask the SFG signature of explosives.

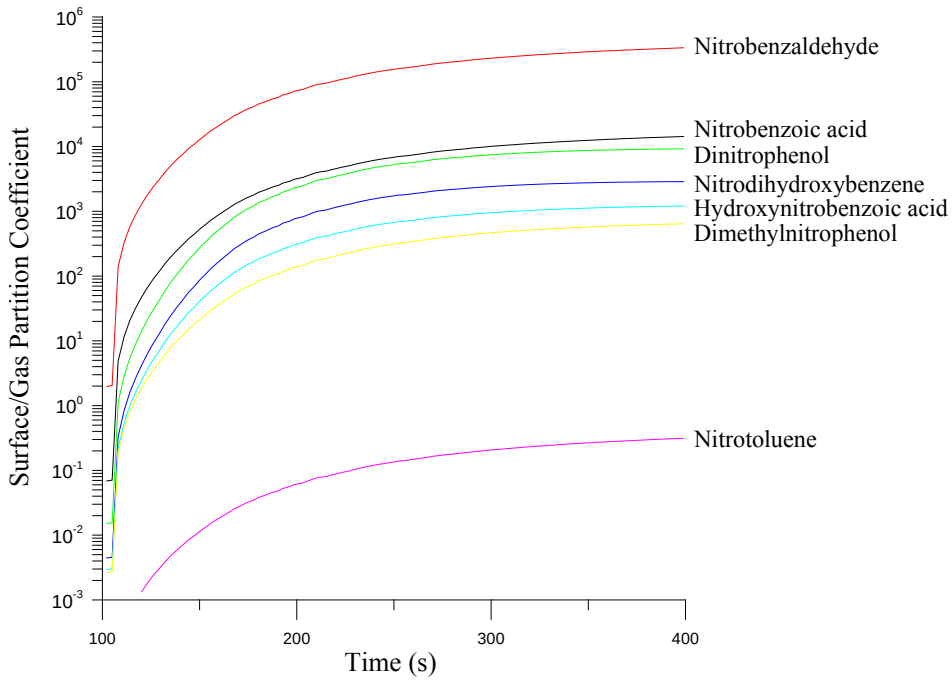

Figure 5. Time series of the surface/gas partition coefficient of several nitro-group containing compounds produced by a photochemical smog model.

10. **Deliverables, Personnel, Awards, Publications, Presentations, and Patents**

Deliverable	Date
Final Technical Report with SF298 (this report)	**January 2011**

Table 1. Deliverables

	Total #	Name	Organization
PIs	1	William Asher	**APL-UW**
Co-PIs	0		
Grad Students	0		
Post Docs	0		
Research Assistants	2	Trina Litchendorf	**APL-UW**
		Andrew Spott	**APL-UW**

Table 2. Personnel Information

	Name	Award (Year Received)	Prize (Year Received)	Recognition (Year Received)
PIs	William Asher	none	none	**none**
Co-PIs	N/A			
Grad Students	N/A			
Post Docs	N/A			
Research Assistants	N/A			

Table 3. Awards/Prizes/Recognitions

Name	Publication (Date)	Conference Presentation (Date)	Patent (Date)
William Asher		Estimating Optical Sum-Frequency Signal Intensities From Trace Levels of Explosives Adsorbed on Surfaces, 7th International Symposium on Mine Warfare (02 May 2006).	

Table 4. Publications, Conference Presentations and Patents

11. **References:**

Asher, W. E., and Spott, A. (2008), The vibrational sum-frequency spectra of films of picric acid, RDX, and TNT on solid surfaces, *J. Molec. Spect.*, *in preparation*.

CREPSEDT (2004) Existing and Potential Standoff Explosives Detection Techniques, 148 pp, National Academy Press, Washington D.C.

Fidric, B. G., et al. (2003), Bananas, explosives and the future of cavity ring-down spectroscopy, *Opt. Phot. News*, *14*, 24-29.

Griffin, R. J., Nguyen, K., Dabdub, D., and Seinfeld, J. H. (2003), A coupled hydrophobic-hydrophilic model for predicting secondary organic aerosol formation, *Journal of Atmospheric Chemistry, 44,* 171-190.

Heinz, T. F., et al. (1983), Determination of Molecular-Orientation of Monolayer Adsorbates by Optical 2nd-Harmonic Generation, *Phys. Rev. A*, *28*, 1883-1885.

Hunt, J. H., et al. (1987), Observation of C-H stretch vibrations of monolayers of molecules optical sum-frequency generation, *Chem. Phys. Lett.*, *133*, 189-192.

Lambert, A. G., et al. (2005), Implementing the theory of sum frequency generation vibrational spectroscopy: A tutorial review, *Appl. Spec. Rev.*, *40*, 103-145.

Shen, Y. R. (1984), *The Principles of Nonlinear Optics*, 612 pp., J. Wiley, New York.

Shen, Y. R. (1999), Surface contribution versus bulk contribution in surface nonlinear optical spectroscopy, *Appl. Phys. B*, *68*(3), 295-300.

Shen, Y. R. (2000), Surface nonlinear optics: A historical perspective, *IEEE J. Sel. Topics Quant. Elec.*, *6*(6), 1375-1379.

Stott, W. R., et al. (1994), Mass spectrometric detection of solid and vapor explosive materials, *Proc. SPIE*, *2276*(Cargo Detection Technologies), 87-97.

Zyss, J. (1993), Engineering new organic crystals for nonlinear optics: from molecules to oscillator, *Journal of Physics D: Applied Physics*, *26*, B198-B207.

Final Report for ONR CODE 30 CIED 6.1 Basic Research Effort

1. **"Distributed Multifunctional Fiber Optic Micro Sensor Arrays for IED Detection"**
2. **Prime Offeror:** University of Washington
3. **Subcontractors:** None
4. **Period of Performance:** August 1, 2005-December 31, 2009
5. **Submitted by:** Antao Chen, antaochen@apl.washington.edu, (206) 543-1274
6. **Business Contact:** Craig Bathgate, Bathgate@apl.washington.edu, 206-543-5437
7. **Background/Scope of Effort**

The goal of this project was to explore the possibility of new sensor materials that change their index of refraction when trace amounts of explosives vapor are present, and the possibility that new fiber optical sensor designs can be fabricated into sensor arrays on a single piece of optical fiber. Such sensors can be placed along roads to detect IEDs at large distances. During the course of the research, new chemo-optic materials that have a significant (> 0.01) change of index of refraction in response to trace amounts of vapor of an explosive simulant (dinitrotoluene (DNT) at 100 parts-per-billion) have been developed. The materials have good selectivity and are insensitive to other chemicals commonly found in the environment, such as salts, chemical fertilizers, and detergents. A new fiber optical sensor concept consisting of micro-ring resonator array fabricated on a flat segment polished onto the surface of the fiber and coupled to the exposed fiber core has been demonstrated in which the micro-ring resonators were made with sensor material. When the fiber optic sensor was exposed to trace amounts of DNT vapor, the resonant wavelengths of the micro-ring resonators shifted toward longer wavelength. The shift of the resonance is reversible and when the sensor is removed from the DNT vapor the resonant wavelengths returned to their original values. In addition to chemo-optic (index changing) sensing materials, we also demonstrated fluorescent-based materials that are responsive to DNT. The micro-resonator sensor elements and fluorescent sensor elements can be co-located on the fiber. Having sensors with different sensing mechanisms would help reduce false detection positives.

The results of this research have been published in several peer-reviewed journal papers and a book chapter, and presented at a number of conferences.

Although the materials we developed have good sensitivity and selectivity, the response times from thin films of these materials are rather slow (a few minutes at best). The response time is limited by the need for the explosive molecules to fully permeate the solid sensing material by diffusion. To achieve a fast response, we explored using a loose mesh of nanowires made of sensing material, and found that a mesh of semiconducting metal oxide nanowires produces both a strong response and a fast response (< 1 second). The goal of the presently funded follow-on project is to understand the fundamental mechanisms of the sensing properties of the semiconducting metal oxide nanowires in order to further improve their sensing properties, with an emphasis on achieving good specificity by surface functionalization of the nanowires.

8. **Summary/Abstract**

Demonstrated a new fiber optical sensor technology that can support a variety of orthogonal sensors by using materials designed to target specific chemicals for IED detection with a low false alarm rate. The proposed technology combines the high sensitivity of optical waveguide resonator sensors and the robustness, low loss, and long range of optical fiber that is excellent for remote activation and interrogation.

Final Report for ONR CODE 30 CIED 6.1 Basic Research Effort

9. Technical Contents and Accomplishments

Through the research of this project we have observed that the vapors of 2,4- and 2,6-dinitrotoluenes (DNT) cause drastic changes in the linear optical properties, e.g., index of refraction and absorption spectrum, of certain chromophore-containing polymer thin films. Figure 1 shows UV-VIS-NIR absorption spectra of a thin film of chromophore DH6[1] (shown in Figure 2) doped in polymethylmethacrylate (PMMA) at 20 wt.% upon exposure to DNT as a function of the duration of exposure. The polymer films were spin coated from solution on glass slides, and dried overnight in vacuum at 60 to 70 ºC. The thickness of the film is 1 μm. The film is not electrically poled and the chromophores are randomly orientated in the matrix of the PMMA host. The main absorption peak originally at 630 nm shows a red shift as large as 70 nm and a reduced peak absorbance from 1.53 to 0.3 after the film is exposed to the analyte vapor saturated in air at 65 ºC for 24 hours. Similar changes have also been observed at room temperature although the same degree of change took place about ten times more slowly. The change of color of the film is also visible to the unaided eye. The color of the polymer film changes from dark blue to light purple. The changes in the absorption spectrum, and the corresponding color changes were observed with a number of host polymers doped at various levels with several different chromophores (DH6[1], AJL8[2], DR1[3]) of the D-π-A structure shown in Figure 2. The type of host polymer (PMMA, amorphous polycarbonate (APC), and bisphenol-A-polycarbonate) and solvent (chloroform and cyclopentanone) used to make the polymer solutions have only a minor effect on the polymer thin film's response to DNT.

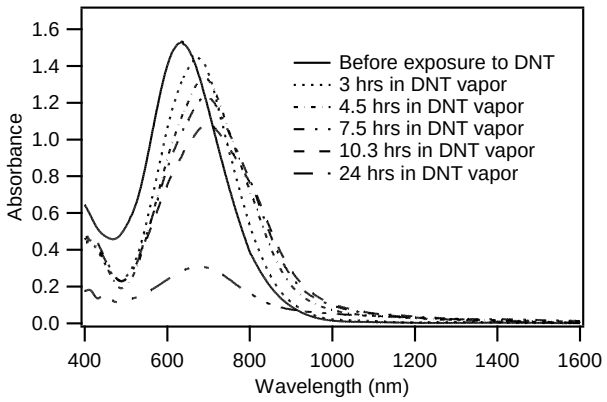

Figure 1. Absorption spectrum of a DH6/PMMA thin film after it is exposed to DNT vapor at 65 ºC for various periods of time. The peak at about 630 nm is the characteristic absorption peak of the chromophore.

Accompanying the change in the absorption spectrum is a change in the index of refraction. Chromophores of the D-π-A structure are highly polarizable and contribute to the index of refraction of the polymer. The polarizability, and therefore the index of refraction, can be affected by the electric field acting on the chromophore due to the local environment. The local electric field environment can, in turn, be affected by nitroaromatic explosive molecules that are highly electronegative and polar. To study the sensitivity and specificity of the polymer as trace explosive sensor materials, similarly prepared thin films of 20 wt. % AJL8 chromophore in APC host were exposed to saturated vapors of DNT and to other chemicals that are a common cause of false positives of explosives sensors. These chemicals include pollutants commonly found in the environment, e.g., salts, chemical fertilizers, and detergents. The thin film samples were individually sealed in separate containers with each of these chemicals, and thereby exposed to a

maximum of the saturated vapor concentration of these chemicals at room temperature. The test condition represents the highest possible concentration of each of these chemicals in a natural environment, and therefore it is a meaningful indicator of sensor specificity. The concentration of saturated DNT vapor in air at room temperature is known to be 100-120 parts-per-billion.[4] The index of refraction of these thin film samples was measured at the wavelength of 1550 nm with a prism coupler (Metricon 2010) after various time periods of the exposure to the chemical vapors. Figure 3 shows the index of refraction change of these samples over time. The data show that this polymer has good specificity to DNT. The maximum refractive index change of this polymer is 0.012 at 100-120 ppb of DNT vapor concentration at room temperature. Considering that the index of refraction can be measured with a sensitivity of 10^{-7} with well engineered polymer micro-ring resonators,[5] a detection limit based on the index change of this polymer of 1 part-per-trillion could be achieved. In general, the change in the index of refraction can be measured more accurately than the change in the absorption spectrum, for example, using micro-ring resonators and fiber Bragg gratings. Therefore, sensors based on the refractive index change could be more sensitive than the sensors based on the absorption spectrum change.

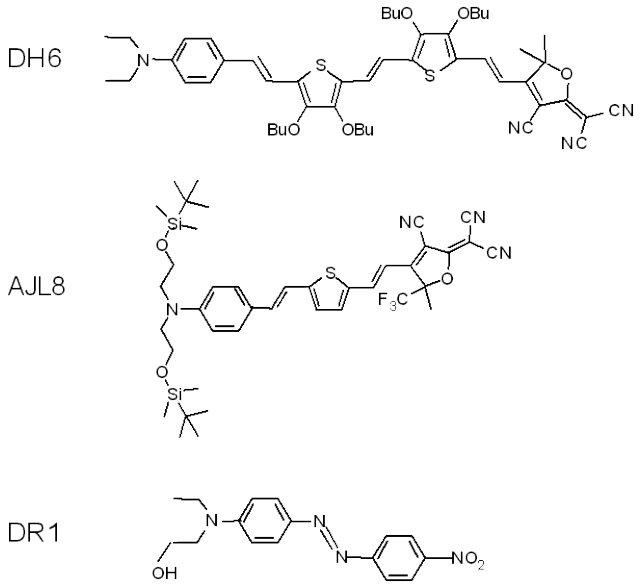

Figure 2. Chemical structures of the chromophores used in this study.

The exact mechanism of how DNT molecules interact with the chromophores in the polymer matrix requires further study. Initial observations suggest that because DNT molecules are highly electron-deficient, chromophores have an electron-rich donor and bridge, and that both DNT and chromophores are highly polar (DNT molecules and chromophores have a strong tendency to interact with each other). Our observation indicates that there are two processes of explosive-chromophore interaction. A relatively fast process is a red-shift of the absorption peak. The height of the absorption peak has little change. This could be due to the fact that DNT molecules create a more polar environment around the chromophores, and the more polar environment leads to a solvatochromic red-shift. The time scale of this process is between several minutes to several hours, depending largely on the permeability of the host polymer. The index and absorption change of the polymer in this process is small and reversible. The second and slower process is the gradual diminishing of the absorption peak. The second process lasts a few hours (in the case of a more permeable polymer DH6 chromophore polydimethylsiloxane) to a few hundred hours

(in the case of a less permeable polymer AJL8 chromophore in amorphous polycarbonate). This indicates that as more DNT molecules migrate to the sites to associate with chromophores, DNT starts to alter the band structure and disrupt the charge transfer bands of the chromophore. The change in the absorption spectra and index of refraction in this process is large and irreversible, an evidence of the strong association between DNT and the chromophore. Such interaction was only observed in solid thin films, and the spectral change does not recover even after the film is subsequently baked at temperatures above 100 ºC for several days, indicating that the interaction between the chromophores and DNT is stronger than the thermal energy. Simply adding DNT to the chromophore solution does not cause any change of the chromophore absorption peak of the solution. This might be because of the overwhelming number of solvent molecules that compete against explosive molecules in interacting with chromophores. Furthermore, if the film that underwent the absorption spectrum change caused by DNT is re-dissolved in the solvent, the absorption spectrum recovers to its original shape, as shown in Figure 4. This reversibility suggests that the interaction between the chromophore and DNT is physical in nature, rather than a chemical reaction. When the film is re-dissolved in the solvent, solvent molecules also interact with the chromphores and compete with DNT molecules. Since solvent molecules in the polymer solution far outnumber DNT molecules, the solvent separates the DNT molecules from the chromophores.

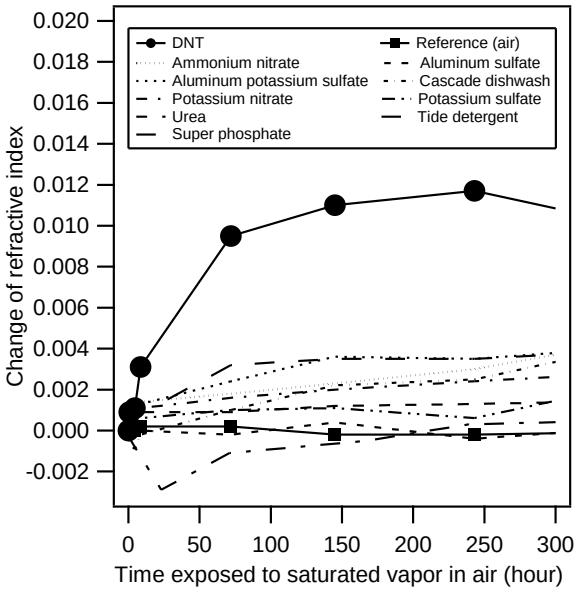

Figure 3. The change of the index of refraction due to DNT is much larger than the change due to other chemicals found in the environment as pollutants. The polymer is 20 wt. % AJL8 chromophore in APC. The index of refraction is measured at the wavelength of 1310 nm. The lines connecting data points in Figures 3 and 5 and the fitted curves in Figures 6 and 8 are only for visual guide.

For the AJL8/APC polymer, saturation was not achieved until 250 hours of exposure to the DNT vapor. However, the sensing polymer produces a detectable amount of refractive index change in approximately ten minutes of exposure to DNT vapor of 100 ppb concentration. The response rate is thought to be limited by the diffusion of DNT molecules into the polymer. When a more permeable polymer, polydimethylsiloxane (PDMS), was used as the host polymer, a ten times improvement in the response rate was observed (Figure 5).

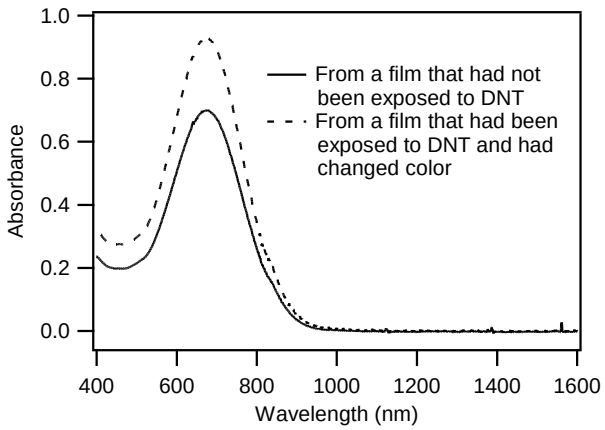

Figure 4. Comparison of the absorption spectra of two DH6/PMMA thin films re-dissolved in cyclopentanone. One is a pristine film without being exposed to DNT and the other is a film that has been exposed to DNT and has changed color. After they are re-dissolved in solvent, the absorption spectra of both samples have the same peak wavelength and shape. The difference in the height of the peak is due to the difference in the concentration of the two polymer solutions.

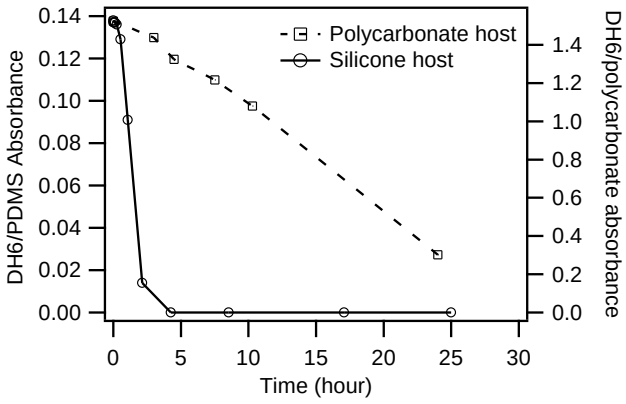

Figure 5. Change of peak absorbance of thin films of DH6 chromophore doped in PDMS and polycarbonate polymer hosts, respectively. PDMS is more permeable than polycarbonate, and produces a more rapid response.

In addition to the intrinsic sensitivity of the sensor material, the overall sensitivity of a sensor can also be greatly enhanced by incorporating optical resonator structures (such as micro-resonators and fiber Bragg gratings) in the sensor design. In these resonators, light at the resonant wavelength makes a large number of passes through the sensor material in the resonator cavity, and therefore the effect of the sensor material on the optical wave is significantly amplified. Micro-ring resonators show great promise for sensor applications because of their sharp resonances and compact size. A wide range of optical signal processing functions, including channel filters, wavelength division multiplexers, switches, dispersion compensators, lasers, polarization rotators, and modulators, can be realized with micro-ring resonators.[6] The resonant properties of micro-ring resonators also makes them an ideal platform for optical sensors.[5] The

small device size makes it possible to integrate a large number of sensors with different functions on the same chip, and also requires a smaller amount of analyte for biological and chemical sensing.

The use of polymer materials offers a number of advantages for making micro-ring resonator devices. With the same waveguide surface roughness, the low refractive index contrast between the polymer waveguide core and cladding (which contributes to the main loss mechanism and compromises the Q-factor of micro-ring resonators) leads to lower scattering loss. Low refractive index and large cross section (for single mode guiding) of the polymer waveguide provide better coupling efficiency to optical fibers, which can significantly reduce the device insertion loss. Device fabrication processes that do not work with other materials may be applicable to polymers. A unique property of chromophore-containing polymers is that optical waveguides and resonators can be fabricated in these polymers through a simple, one-step, dry process termed photobleaching. During photobleaching high energy photons of UV wavelengths decompose the conjugated-electron system of the organic chromophores. This decomposition bleaches out the color of chromophores, reduces the polarizability and the index of refraction of the chromophore-containing optical polymer. Photobleaching has been used to make channel waveguides[7,8] and to perform post-fabrication trimming[9] of polymer waveguide devices. Photobleaching is a single step process, which not only simplifies the device fabrication, but also reduces the sources of error from multiple fabrication steps. Photobleaching also doesn't involve wet chemistry, which may not be compatible with chromophore-containing polymers.

The polymer used in this study was amorphous polycarbonate (APC) doped with 25 wt. % of AJL8 chromophore.[2] Figure 6 gives the refractive index after various doses of photobleaching, indicating a permanent and stable change in the material. The refractive index was measured at the wavelength of 1550 nm, and the photobleaching was carried out using a mercury discharge lamp with emission peaks at 365 nm and 402 nm. The photobleached film loses its dark blue color and becomes completely clear and colorless. It also loses the sensitivity to DNT vapor. An index of refraction decrease of as much as 0.066 is observed after the color of the polymer film is completely bleached out.

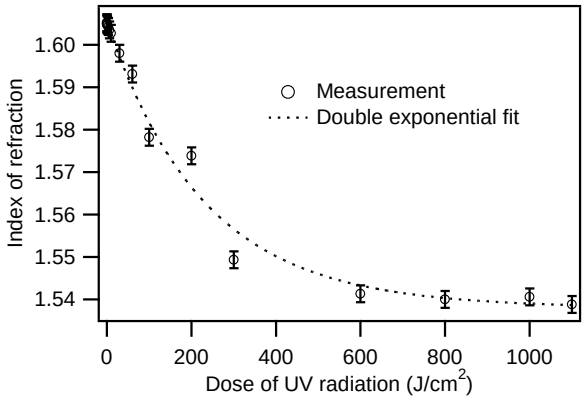

Figure 6. The refractive index of AJL8/APC film showing the change after the film is photobleached at various doses.

Photobleaching also reduces the thickness of the EO polymer by a few percent. This is because some of the photodecomposition products are gaseous and leave the polymer thin film, reducing

the volume of the solid polymer. The photobleached region has the same level of surface smoothness as the unbleached region. Waveguide losses were measured by the cut-back method.[10] The propagation loss was found to be 2.3 dB/cm and 2.0 dB/cm for the TE and TM polarizations, respectively. These are similar to the losses of the ridge waveguides made from the same material by photolithography and reactive ion etching (RIE), which are conventional methods to make waveguides in polymer thin films. Coupling loss from the fiber to the waveguide was 4 dB for each coupling interface, which is a typical value for the polymer waveguides with the same mode size.

Based on these measurement and simulation results, racetrack-shaped micro-ring resonators were designed with a 4-μm wide waveguide, 80 μm coupling length, and 200 μm radius. Samples with coupling gaps ranging from 0.6 to 1.2 μm were tested. It was found that resonators with a coupling gap of 1.1 μm had the highest extinction ratio. Extinction ratios larger than 10 dB can be routinely obtained (Figure 7). The free spectral range between adjacent resonances was approximately 1.08 nm, which is in good agreement with a theoretical calculation. The Q factor of the resonators obtained from curve fitting is in the range of 6500 to 8100 and is adequate for sensor applications. The insertion loss at the peak transmission was 8.7 dB, mainly attributed to the fiber-waveguide coupling.

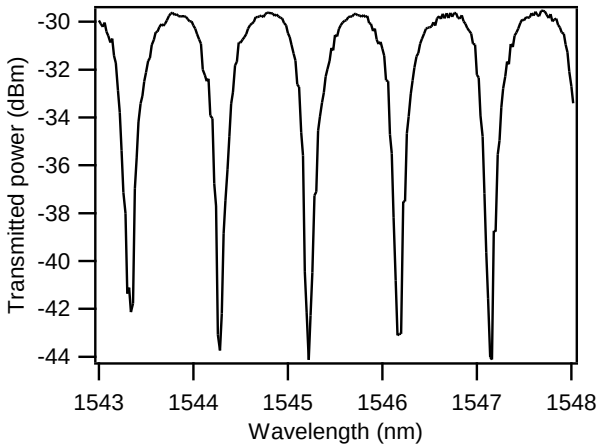

Figure 7. Measured transmission spectrum of a micro-ring resonator made in AL8/APC by photobleaching. The width of the waveguide is 4 μm. The coupling gap is 1.1 μm and the length of the coupling region is 80 μm.

The micro-ring resonators of the 25 wt. % AJL8/APC polymer fabricated with photobleaching were exposed to the saturated DNT vapor at room temperature. A resonance shift towards longer wavelength was observed (Figure 8(a)), indicating an increase in the refractive index of the polymer consistent with the thin-film refractive index measurement results. This response originates from the change of the index of refraction of the core of the channel waveguide, which was shielded by the metallic pattern of the photomask and not photobleached. After one hour of exposure the shift was 1.2 nm and the maximum effect had not yet been reached. After removing the sensor from the DNT atmosphere, the sensor properties returned to their initial conditions (Figure 8(b)). Our current test setup can measure the resonant wavelength to an accuracy of ±0.05 nm. This accuracy corresponds to an accuracy of ±0.00005 for index of refraction measurements, and a sensitivity of ~5 ppb. Sensitivity at this level is comparable to explosive sensors based on fluorescence quenching, which are also typically tested at ppb levels. Unlike sensors based on fluorescence quenching and lasing action, the sensors of this work do not require the use of short

wavelength excitation that can photobleach the sensor materials. Polymer micro-ring resonators with optimized design and fabrication conditions have demonstrated an index of refraction measurement accuracy of 10^{-7}, which corresponds to a detection sensitivity of a few parts-per-trillion (ppt).

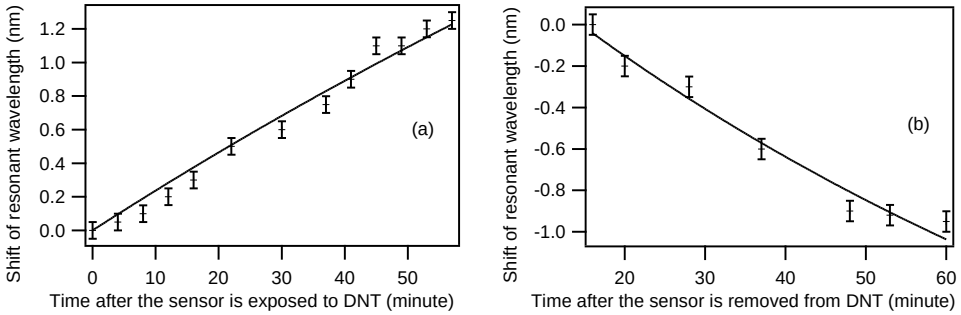

Figure 8. The output of the sensor when it is exposed to, (a), and removed from, (b), saturated DNT vapor at room temperature.

In conclusion, chromophore-containing polymers also have potential applications in sensors to detect trace vapor of common explosives. Novel trace explosives sensors using chromophore-containing polymers have been successfully demonstrated. A photobleaching technique is capable of fabricating high quality micro-ring resonators in chromophore-containing polymers, which can be used to detect trace explosives. Detection sensitivity of DNT at ppb level with good specificity has been demonstrated, and polymer detectors have the potential of pushing the detection limit to the ppt level. The response time of the sensing polymers is limited by the diffusion of the explosive molecules to permeate polymer thin film, and more permeable thin films can lead to faster responses.

10. **Deliverables, Personnel, Awards, Publications, Presentations, and Patents**

Deliverable	Date
"Trace explosive sensor using nanostructured chemoresistive thin film," A. Chen, D. Wang, Q. Zhang, and G. Cao, University of Washington TechTransfer Reference Number 8049D, April 17, 2008.	**17 April 2008**
Final Technical Report (this report)	**January 2011**

Table 1. Deliverables

Final Report for ONR CODE 30 CIED 6.1 Basic Research Effort

	Total #	Name	Organization
PIs	1	Antao Chen	Applied Physics Lab, University of Washington
Co-PIs	2	Larry Dalton	Chemistry Department, University of Washington
		Alex K.-Y. Jen	Materials Science and Engineering Department, University of Washington
Grad Students	2	Anna Pyayt	Electrical Engineering Department, University of Washington
		Haishan Sun	Electrical Engineering Department, University of Washington
Post Docs	0		

Research Assistants	2	Anna Pyayt	Electrical Engineering Department, University of Washington
		Haishan Sun	Electrical Engineering Department, University of Washington

Table 2. Personnel Information

Final Report for ONR CODE 30 CIED 6.1 Basic Research Effort

	Name	Award (Year Received)	Prize (Year Received)	Recognition (Year Received)
PIs	Antao Chen	Applied Physics Laboratory Science and Engineering Award. (2006).		
Co-PIs	Alex K.-Y. Jen	Faculty of Research Innovator Award, College of Engineering, University of Washington, (2007).		Fellow, American Chemical Society, Polymeric Materials, Science & Engineering, (2009)
				Fellow, Optical Society of America, (2007)
				Fellow, The International Society of Optical Engineering (2006)
Grad Students	Anna Pyayt	Society of Women Engineers' Outstanding Female Award (2007).	Microsoft Research Fellow (2007, 2008).	
		Department of Electrical Engineering Chair's award (2006).	SPIE Educational Scholarship in Optical Science and Engineering four times in a row (2006, 2005).	
Post Docs				

Research Assistants				

Table 3. Awards/Prizes/Recognitions

Final Report for ONR CODE 30 CIED 6.1 Basic Research Effort

Name	Publication (Date)	Conference Presentation (Date)	Patent (Date)
Antao Chen, Haishan Sun, Anna Pyayt, and Xunqi Zhang, Jingdong Luo, Alex Jen, Philip A. Sullivan, Samy Elangovan, Larry R. Dalton, Raluca Dinu, Danliang Jin, and Diyun Huang	"Chromophore-containing polymers for trace explosive sensors," *Journal of Physical Chemistry C* **112**, 8072–8078 (2008).		
Antao Chen, Larry R. Dalton and Anna Pyajt, Jingdong Luo, Steven Hau, and Alex K-Y Jen		"Fiber Optic Sensor Based on Conjugated Molecules for IED Detection," presented at the 7th International Symposium on Technology and Mine Problem, Monterey, CA, May 2-5, 2006.	
Antao Chen, Danling Wang, and Gouzhong Cao			Patent application "Detection of trace chemicals and method therefor," application number PCT/US2009/046157, filed on June 3, 2009.
Antao Chen, Haishan Sun, Anna Pyayt, Jingdong Luo, and Alex K.-Y. Jen	"Micro-ring resonators made in poled and un-poled chromophore-containing polymers for optical communication and sensors (Invited)," *IEEE Journal of Selected Topics in Quantum Electronics* **14**, 1281–1288 (2008).		

Antao Chen	Book chapter. Chapter 2, "Microresonator sensors made in polymers with functional chromophore dopants," in *Advanced Photonic Structures for Biological and Chemical Detection*, Xudong Fan ed., Springer, New York, pp. 7-34 (2009).		
W. C. Wu, Y. Tian, C. Y. Chen, C. S. Lee, Y. J. Sheng, W. C. Chen, and A. K.-Y. Jen	"Theoretical and Experimental Studies on the Surface Structures of Conjugated Rod-Coil Block Copolymer Brushes," *Langmuir* **23**, 2805-2810 (2007).		
C-C. Yang, Y. Q. Tian, C. Y. Chen, A. K.-Y. Jen, and W.-C. Chen	"A Novel Benzoxazole-containing Poly(N-isopropylacrylamide) Copolymer as Multifunctional Sensing Materials," *Macromol. Rapid Commun.* **28**, 894-896 (2007).		
L. Fang, J. Y. Park, H. Ma, A. K.-Y. Jen, and M. Salmeron	"An atomic force microcopy study of the mechanical and electrical properties of monolayer films of molecules with aromatic end groups," *Langmuir* **23**, 11522-11528 (2007).		
Haishan Sun, Anna Pyajt, Jingdong Luo, Zhengwei Shi, Steven Hau, Alex Jen, Larry Dalton, and Antao Chen	"All-dielectric electro-optic sensor based on polymer micro-resonator coupled side-polished optical fiber," *IEEE Sensors Journal* **7**, 515-524 (2007).	.	
Haishan Sun and Antao Chen		"Multiple Slot Waveguides for Enhanced Biochemical Sensing," 2009 IEEE/LEOS	

		International Conference on Optical MEMS and Nanophotonics, 17-20 August 2009, Clearwater Beach, Florida.	
Haishan Sun, Antao Chen, and Larry R. Dalton	"A reflective microring notch filter and sensor," *Optics Express* **17**, 10731–10737 (2009).		
Anna Pyayt, Jun Zhou, Antao Chen, Jingdong Luo, Steven Hau, Alex Jen, and Larry Dalton		"Electro-optic polymer microring resonators made by photobleaching," *Proceedings of SPIE*, vol. 6470, pp. 64700Y:1-7 (2007).	
Anna Pyayt, Xuanqi Zhang, Jingdong Luo, Alex Jen, Larry Dalton, and Antao Chen		"Optical micro-resonator chemical sensor," *Proceedings of SPIE*, vol. 6556, pp. 65561D:1-6 (2007).	

Table 4. Publications, Conference Presentations and Patents

11. **References:** (In support of Sections 7-9 above.)

1. Jin, D.; Londergan, T.; Huang, D.; Wolf, N.; Condon, S.; Tolstedt, D.; Guan, H.W.; Cong, S.; Johnson, E.; Dinu, R. *Proc. SPIE* **2004**, *5351*, 44.
2. Luo, J.; Liu, S.; Hailer, M.; Kang, J. –W.; Kim, T. –D.; Jang, S. –H.; Chen, B.; Tucker, N.; Li, H.; Tang, H. –Z.; Dalton, L. R.; Liao,Y.; Robinson, B. H.; Jen A.K.Y. *Proc. SPIE* **2004**, *5351*, 36.
3. Samoc, A.; Samoc, M.; Luther-Davies, B.; Kolev, V.Z.; Bagien, R.K.; Luo, X.; Zha, C. *Molecular Crystals and Liquid Crystals* **2006**, *446*, 123.
4. Jose, A.; Zhu, Z.; Madigan, C.F.; Swager, T.M.; Bulovic, V. *Nature* **2005**, *434*, 876.
5. Chao, Ch.-Y.; Fung, W.; Guo, L. J. *IEEE Journ. Select. Topics in Quant. Electr.* **2006**, *12*, 134.
6. Little, B. E.; Chu, S. T. *Optics & Photonics News* **2000**, 24.
7. Ma, J.; Lin, S.; Feng, W.; Feuerstein, R.J.; Hooker, B.; Mickelson, A. R. *Appl. Opt.* **1995**, *34*, 5352.
8. Zhou, J.; Pyayt, A.; Dalton, L.R.; Luo, J.; Jen, A.K.Y.; Chen, A. *IEEE Photon. Technol. Lett.* **2006**, *21*, 2221.
9. Chen, A.; Chuyanov, V.; Marti-Carrera, F. I., Garner, S.; Steier, W. H.; Mao, S. S. H.; Ra, Y.; Dalton, L. R.; Shi, Y. *Photon. Techno. Lett.* **1997**, *9*, 1499.
10. Nordstrom, M.; Zauner, D.A.; Boisen, A.; Hubner, J. *J. Lightwave Technol.* **2007**, *25*, *1284.*

Final Report for ONR CODE 30 CIED 6.1 Basic Research Effort

1. **"Deep Bleeder Mitigation by Image Guided Ultrasound"**
2. **Prime Offeror:** Applied Physics Laboratory, University of Washington
3. **Subcontractors:** None
4. **Period of Performance:** 08/01/2005 – 12/31/2009
5. **Submitted by:** Lawrence A. Crum, lac@apl.washington.edu, 206-685-8622
6. **Business Contact:** Monty Bolstad, monty@apl.washington.edu, 206-543-9826

7. **Background/Scope of Effort**

This effort was part of a larger program at the Applied Physics Laboratory at the University of Washington in Seattle. Work specific to the deep bleeder mitigation project was conducted in collaboration with Dr. Stephen J. Carter of the UW Radiology Department.

8. **Summary/Abstract**

The major goals of this effort were as follows: (1) Adapt and modify an image-guided High Intensity Focused Ultrasound (HIFU) device for use in an investigation of acoustic hemostasis; (2) perform *in vitro* laboratory studies of this device; (3) perform *ex vivo* studies of HIFU-induced temperature elevation; (4) perform *in vivo* studies of visible bleeding; (5) perform *in vivo* studies of occult bleeding; and (6) develop and treat a realistic porcine model of retro-hepatic bleeding. These goals, if accomplished would lay the framework for the development of a hand-held, image-guided, acoustic hemostasis device that could be used to stop bleeding in injured combatants.

9. **Technical Contents and Accomplishments**

Many of the original goals were accomplished; unfortunately, this effort was not continued beyond the initial phase and therefore no device was developed that was suitable for transition to clinical unit sufficient for regulatory approval and human clinical trials. We report below some of the accomplishments of the effort. In our studies, we successfully obtained both *in vitro* and *in vivo* results of the application of HIFU to pig arteries, and specifically concentrated on histology and biochemistry. Our results show that even when significant histological damage is observed during treatment, the *in vitro* biochemistry is significantly different from that for the *in vivo* case. These studies demonstrate the importance of *in vivo* studies when examining the ability of HIFU to induce acoustic hemostasis.

Major Achievements: We describe in some detail a few major achievements of this research; significant progress was made toward our major research goals.

In vitro studies: An *in vitro* perfusion flow system was designed in order to evaluate the effects of HIFU on blood alone (within a plastic tube), and within a freshly excised porcine vessel. During circulation, the flow rate was maintained at a physiological rate of 80 ml/min and mean pressure of 60 mmHg. The target (tube or excised vessel) was sandwiched between muscle tissues in order to more closely mimic the *in vivo* setting. Blood was either static or circulating during treatment, and was removed immediately pre and post treatment for the biochemical analysis. Treatments were performed using a custom built image-guided HIFU therapy system. For all treatments, no significant change in the concentration of fibrinolysis markers (tissue plasminogen activator, tPA and plasminogen activator inhibitor type 1, PAI-1) or coagulation markers (thrombin/anti-thrombin complex, TAT and fibrinopeptide, FPA) was observed.

In vivo studies: An *in vivo* non-injury model was used to determine the effects of the HIFU on blood. Domestic swine (40-50 kg) were anesthetized and instrumented to monitor heart rate, oxygen saturation (SpO_2), blood pressure, and core temperature. The lower abdomen was depilated and wiped with 70% isopropanol before the vessel (common femoral and superficial)

characteristics (diameter, flow, peak systolic velocity) were measured by a sonographer. A skin flap was made and the vessels exposed in order for them to be instrumented with flow probes and thermocouples. A catheter was placed in the superficial artery to facilitate the blood draw. After instrumenting, the cavity was filled with saline and the flap was closed. Image-guided transcutaneous treatments were performed on the vessels using a custom built image-guided HIFU therapy system with a 2 MHz, 8 element phased array. Total HIFU treatment lasted 8 seconds and a range of acoustic intensities and duty factors were evaluated. Blood was removed immediately pre and post treatment for analysis.

There was no significant change in CBC (Complete Blood Count), blood chemistry (Na^+, K^-, pCO_2) or ACT (Activated Clotting Time) observed post treatment compared to pre treatment. However, there was a significant increase in the coagulation markers TAT and FPA ($p < 0.05$, $n = 9$) at the high intensity level (80 W/cm^2). In addition the fibrinolysis marker tPA was found to increase post treatment ($p < 0.05$, $n = 5$) with a high duty factor (50%), but decreased post treatment ($p < 0.05$, $n = 5$) with the low duty factor (30%). No significant change was observed in the PAI-1 levels post treatment. These data are shown in Figs. 1A and 1B below:

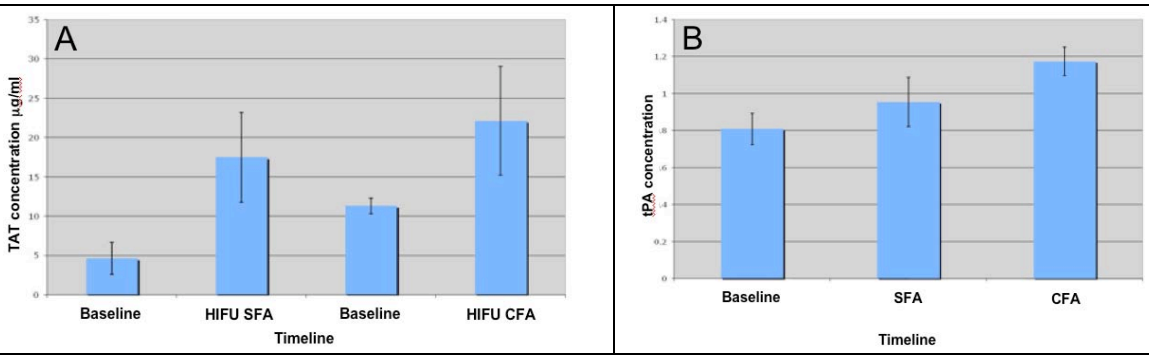

Fig. 1. tPA concentration after HIFU treatment of pig superficial(SFA) and common(CFA) femoral arteries.

Histologically, damage to the endothelium in the area of treatment could be observed in many of the treated vessels, as shown in Fig. 2. In all cases damage was localized and no collateral damage was observed. However, no correlation can yet be drawn between vessel damage and the treatment type. The discrepancy observed between the *in vitro* and *in vivo* results could be due to the use of heparin in the blood to prevent thrombosis. The decrease in thrombin generation results in the subsequent decrease in TAT complex and FPA formation. It is possible that the heparin concentration could be adjusted allowing for the physical use of the blood whilst maintaining it hematologically 'active.' Further studies are needed to determine this concentration. The significant increases in TAT and FPA *in vivo* observed post treatment, at the high intensity level (80 W/cm^2), confirms the presence of thrombotic events and the enhanced activity of thrombin resulting from the HIFU. At the higher duty factor (50%), a significant increase in tPA was observed post treatment which suggests the presence of fibrinolysis. The increase in coagulation factors could be explained by damage to the endothelium, platelet activation or enzymatic protein alteration leading to increased proteolytic processes. The fact that no significant increase in any coagulation or fibrinolysis marker at the lower intensities and lower duty factors suggests that HIFU parameters can be tailored to elicit specific responses from the endothelial cells and blood depending on the desired end result (i.e., coagulation/hemostasis without damaging surrounding tissue).

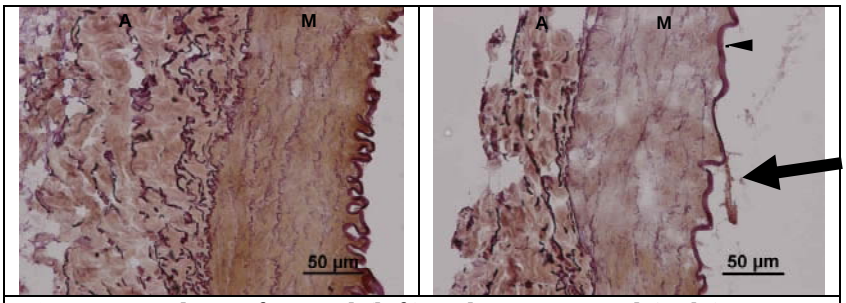

Fig. 2: Histology of control (left) and HIFU-treated (right) arteries. Modified Harts' staining (elastin is black) of the right common femoral artery illustrating the change in endothelium after treatment. Treated artery has no digitations in the endothelium (arrow) and the extracellular matrix in the tunica media (M) as well as the tunica adventitia (A) is not as organized.

Studies of retro-hepatic bleeding: Perhaps our major accomplishment was the demonstration of the detection, localization, and termination of retro-hepatic bleeding in a porcine model in collaboration with Army trauma surgeons at Tripler Army Medical Center in Honolulu, Hawaii. In our conversations with trauma surgeons who had served in Iraq, they indicated that a common condition that challenged them in the operating room was the relatively common occurrence of retro-hepatic bleeding. When an IED would explode in the vicinity of a soldier, the blast wave would cause trauma to the liver, which would often fracture and bleed. Treating bleeding in open surgery is difficult enough, but when it occurs in the back of the liver, it is nearly impossible to treat. Lifting the liver will exacerbate fractures and tears; thus, the only treatment is to pack the liver and wait to see if coagulation will occur naturally. Our approach was to use the image-guided acoustic hemostasis device to target the bleeding site and into hemostasis. Some results are shown in Fig. 3

.

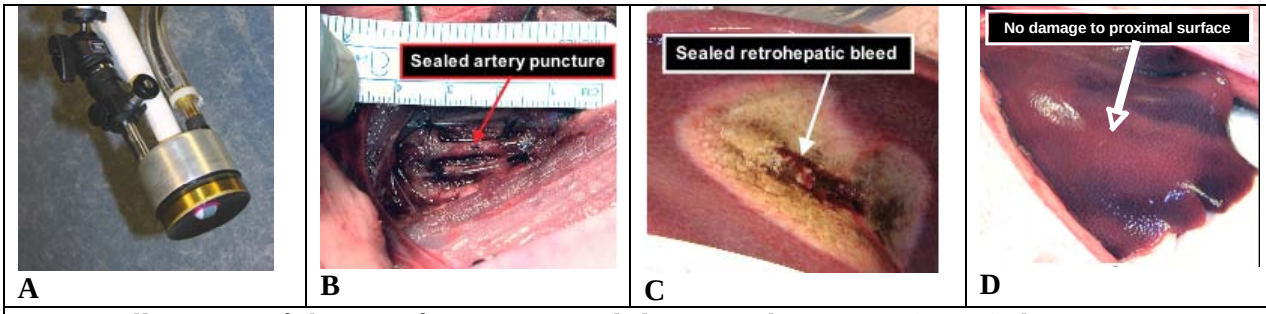

Fig. 3. Illustration of the use of our image-guided acoustic hemostasis (IGAH) device to treat retro-hepatic bleeding in a porcine model. Shown in A is the integrated image-guided HIFU device, comprised of an imaging probe and an annular HIFU array. Shown in B is a photograph of the sealed artery that was targeted with the IGAH device; in C is the tissue in the back of the liver, and in D the tissue in the front of the liver–indicating no damage to this side.

Conclusions: These results demonstrate the potential utility of such a device in the treatment of trauma in injured combatants.

10. **Deliverables, Awards, Publications, Presentations, and Patents:** none

11. **References:** none

Final Report for ONR CODE 30 CIED 6.1 Basic Research Effort

1. **"Forensic Analysis of Explosive Materials Using X-ray Emission Spectroscopy"**
2. **Prime Offeror:** University of Washington
3. **Subcontractors:** None
4. **Period of Performance: 8/01/2005 to 12/31/2009**
5. **Submitted by:** W. T. Elam, wtelam@apl.washington.edu, 202-685-3092
6. **Business Contact:** Monty Bolstad, monty@apl.washington.edu, 206-543-9826

7. **Background/Scope of Effort** This project has two components: forensic analysis of explosives using the direct X-ray emission of the carbon, nitrogen, and oxygen atoms in explosives; and investigation of a new, unique approach to standoff explosives detection. All chemical explosives store energy in specific, high-energy chemical bonds. Detecting and classifying explosives is a matter of analyzing the structure of these bonds by some method, either direct or indirect. One direct method is to measure the X-ray emission spectrum (XES) of the relevant elements involved in the chemical bonds (such as nitrogen or oxygen in a typical explosive). XES involves electron transitions between an atomic core state and the filled bonding states. The detailed shape of XES lines reflects the chemical bonding of the element whose characteristic emission lines are observed. Each element in the periodic table emits X-rays at characteristic energies. The overall intensity of the emission lines is proportional to the amount of the element present and the shape is related to the chemistry. Thus XES provides chemical information about both composition and bonding. A complementary technique to XES is provided by a particular type of non-resonant inelastic X-ray scattering (NRIXS). The inelastic scattering from the core shell electrons of low-Z elements such as nitrogen can be readily detected by synchrotron-based NRIXS at photon energies of 10 keV. This scattering also provides information about the local chemical environment of the nitrogen species. If NRIXS can make chemical information accessible in a standoff situation at the X-ray energies used for backscatter imaging, it could be used in combination with imaging to reduce false alarm rates. This would lead to a reliable and adaptable standoff detection method. Backscatter imaging with subsequent single-spot chemical information from NRIXS would be a very powerful combination for a standoff sensor, since the image and chemistry provide orthogonal information about the device. Investigations into the utility of forensic efforts in-country led to the conclusion that current forensics techniques were adequate and there was no compelling need for new forensics methods. As a result, the effort under this project shifted from the forensics task to the standoff detection task. While the standoff detection method being explored was high risk, it was deemed a more pressing need and justified pursing high risk research.

8. **Summary/Abstract** The goals of this project were to modify the existing FEFF 8 solid-state theory computer code [1] to allow calculation of the X-ray emission spectrum (XES) of nitrogen and other elements in explosive compounds. The XES of nitrogen in various explosives as well as similar non-explosive compounds would be calculated using this modified code. This would enable identification of the features in the XES that are associated with explosive chemistry. A limited set of measurements would be taken at a synchrotron source to verify the calculations. A second set of goals was to calculate the magnitude of the non-resonant X-ray inelastic scattering (NRIXS) cross section and verify the calculations with a limited set of measurements at both synchrotron light sources and with laboratory X-ray sources. This cross section would then be used to calculate the size of the NRIXS signal for some typical backscatter imaging geometries.

9. **Technical Contents and Accomplishments** Non-resonant X-ray emission spectroscopy was used to compare the nitrogen-rich compounds ammonium nitrate, trinitrotoluene, and cyclotrimethylene-trinitramine. They are representative of crystalline and molecular

structures of special importance in industrial and military applications. The spectral signature of each substance was analyzed and correlated with features in the electronic structure of the systems. This analysis was accomplished by means of theoretical simulations of the emission spectra and a detailed examination of the molecular orbitals and density of states. We find that the two theoretical methods used ("frozen-orbital" density functional theory [2] and real-space Green's function simulations [1]) account semi-quantitatively for the observed spectra and are able to predict features arising from distinct chemical complexes. A comparison of the calculations and the data provides insight into the electronic contributions of specific molecular orbitals, as well as the features due to band-like behavior. With some additional refinements, these methods could be used as an alternative to reference compounds. Features observed in XES and XRF have the added advantage that they can be measured in spectra produced when electron microscopes or X-ray tubes create the required core-holes. Thus, details observed under conditions of selective excitation and high resolution can frequently supply insight in widespread applications, even those resulting in spectra of lower resolution and intensity.

The incident X-rays in Non-resonant inelastic X-ray scattering (NRIXS) can have very high energies and therefore can penetrate many materials (such as suitcases, soil, etc.). The binding energies investigated, however, are at energies comparable to the Compton shift, which is much less than the incident energy. This allows access to the electronic transitions of the light elements, such as carbon, nitrogen, and oxygen that are typical components of explosives. The electronic binding energies of these light elements are below 1 keV. X-rays of this low energy cannot penetrate air for any significant distance. The unique combination of penetrating power and chemical information about light elements makes NRIXS a good candidate for finding and identifying explosives within containers, buildings, or other concealment. NRIXS, however, is a weak effect. To investigate the feasibility of using NRIXS to detect and identify explosives, we have predicted the signal to noise from NRIXS for typical applications. To achieve this, a new Atomic Inelastic X-ray Scatter (AXIS) computer code was developed, tested, and its accuracy verified by synchrotron and laboratory measurements.

First, we measured the NRIXS spectrum of selected compounds using a synchrotron source. The use of a synchrotron provides a strong signal and thus very good signal to noise at very high measurement resolution (better than 1 eV). This yields very good data to evaluate NRIXS and make comparisons to calculations. Second, we developed a computer code to calculate the size and chemical dependence of the NRIXS scatter cross-section. This new code was named AXIS for Atomic X-ray Inelastic Scatter code. AXIS incorporates a fundamental parameters code to include the effects of self-absorption, absorption in the air path and any other obstructions, and geometry. An algorithm to calculate the absolute output of an X-ray tube was also included. This gives an absolute calculation of the rate of photons expected in the detector. The calculations were validated using the synchrotron data and additional data collected in the laboratory. The laboratory data did not have the energy resolution to determine chemical effects, but it did validate the absolute intensity of the scatter and the absolute output of the X-ray tube. These validations were important in establishing the reliability of the signal strength predictions. Finally, we calculated the signal strength for a number of relevant geometries. These geometries were based as closely as could be approximated to application scenarios expected in the field. One scenario focused on typical suitcase inspection that may occur in airports while a second scenario focused on standoff detection from a vehicle.

The AXIS calculations were absolute in that no adjustable parameters were employed and the actual observed intensity of the signal was predicted. Calculation accuracy was verified by comparison with high-resolution synchrotron measurements as well as laboratory measurements with more realistic sources. Agreement of the absolute signal was within 40% relative error at worst and often much better. AXIS simulations of several scenarios where explosives detection and identification are encountered were also performed. Our AXIS simulation shows that a suitcase or package inspection system based on non-resonant inelastic X-ray scattering is clearly feasible with existing technology plus some enhancements that are fairly straightforward. AXIS simulation of a standoff inspector indicates feasibility for distances somewhere between 10 and 100 m with emerging technology that is as yet untested. Standoff detection via this approach is limited to situations were the scatter angle can be 20 degrees or less. Additional details of these investigation are available in the references listed below and included via hyperlink in this report.

10. **Deliverables, Personnel, Awards, Publications, Presentations, and Patents**

Deliverable	Date
"Predicting the Utility of Non-Resonant Inelastic X-ray Scattering (NRIXS) for Standoff Explosives Detection," W. T. Elam, G. Seidler, T. Fister, K. Nagel, and L. Buck, University of Washington Applied Physics Laboratory Technical Report 0903, November 2009.	**November 2009**
"Method of detecting, identifying, and quantifying bulk, light-element materials using high-energy, penetrating X-rays," W. T. Elam , L. J. Buck, G. T. Seidler, and T. T. Fister, Record of Invention, University of Washington TechTransfer Reference Number 7899D, October 10, 2007.	**10 Oct 2007**
Final Technical Report (this report).	**January 2011**

Table 1. Deliverables

Final Report for ONR CODE 30 CIED 6.1 Basic Research Effort

	Total #	Name	Organization
PIs	1	W. T. Elam	**Univ. of Washington APL**
Co-PIs	1	Gerald T. Seidler	**Univ. of Washington Physics Dept.**
Grad Students	2	Timothy Fister	**Univ. of Washington Physics Dept**
		Kenneth Nagel	**Univ. of Washington Physics Dept**
Post Docs	1	Fernando Vila	**Univ. of Washington Physics Dept**
Research Assistants	0		

Table 2. Personnel Information

	Name	Award (Year Received)	Prize (Year Received)	Recognition (Year Received)
PIs	W. T. Elam			Appointed to Advisory Board, *X-ray Spectrometry* (2007)
				Elected to membership, International Centre for Diffraction Data (2008)

Table 3. Awards/Prizes/Recognitions

Name	Publication (Date)	Conference Presentation (Date)	Patent (Date)
T. T. Fister, G. T. Seidlera, L. Wharton, A. R. Battle, T. B. Ellis, J. O. Cross, A. T. Macrander, W. T. Elam, T. A. Tyson, and Q. Qian	"Multielement Spectrometer for Efficient Measurement of the Momentum Transfer Dependence of Inelastic X-ray Scattering," *Review of Scientific Instruments* **77**, 063901:1-7 (□2006).		
T. Jach, J. N. Ullom, and W. T. Elam		"The microcalorimeter X-ray detector: A true paradigm shift in X-ray spectroscopy," *Eur. Phys. J. Special Topics* **169**, 237–242 (2009).	
T. T. Fister, G. T. Seidler, J. J. Rehr, J. J. Kas, W. T. Elam, J. O. Cross, and K. P. Nagle,	"Deconvolving Instrumental and Intrinsic Broadening in Core-shell X-ray Spectroscopies," *Physical Review* **B 75**, 174106:1-10 (□2007).		
F. D. Vila, T. Jach, W. T. Elam, J. J. Rehr, and J. D. Denlinger	"X-ray emission spectroscopy of nitrogen-rich compounds" (draft, October 5, 2009).		

Table 4. Publications, Conference Presentations and Patents

11. **References:** (In support of Sections 7-9 above.)

1. A. L. Ankudinov, B. Ravel, J. J. Rehr, and S. D. Conradson, "Real-space multiple-scattering calculation and interpretation of x-ray-absorption near-edge structure," *Phys. Rev.* ***B*** **58**, 7565-7576 (1998).
2. L. Triguero, L Pettersson, and H. J. Agren, "Calculations of X-ray Emission Spectra of Molecules and Surface Adsorbates by Means of Density Functional Theory," *Phys. Chem.* ***A*** **102**, 10599-10607 (1998).

Final Report for ONR CODE 30 CIED 6.1 Basic Research Effort

1. **"Similarity-Based Statistical Learning Architecture for IED Prediction and Detection"**
2. **Prime Offeror:** University of Washington, Seattle, WA, USA
3. **Subcontractors:** N/A
4. **Period of Performance: August 1, 2005 to December 31, 2009**
5. **Submitted by:** Maya Gupta, gupta@ee.washington.edu, 206-543-0478
6. **Business Contact:** Andrei Stabrovski, andreis@u.washington.edu, 206-685-1979

7. **Background/Scope of Effort** : IEDs are funded, built, and placed by humans. Humans follow patterns, and despite their best efforts, will be forced to follow patterns under the pressures and limited resources of a conflict. Pattern recognition will be useful to predict IEDs, detect IEDs, provide intuition for troops to assess risk from IEDs, and predict decoys. Current pattern recognition approaches, however, will not perform well on the difficult problem of IED prediction and analysis. In particular, one will have only a few examples of IEDs, and the sought-after patterns must be discovered from a large set of disparate data streams that may include cell phone activity, hearsay intelligence, chemical sensors, detected movements, etc. We propose basic research into a new statistical learning architecture that can recognize patterns from small numbers of samples and effectively fuse many disparate data sources by using flexible set-based similarity measures based on psychology and information theory. The resulting identified patterns and classifications would empower troops with analysis and intuition to make real-time decisions.

8. **Summary/Abstract** The first primary research objective was to develop quantitative similarity measures that can better handle high-dimensional data, noisy data, non-numerical data, missing data, and variables whose predictive value is uncertain. The second primary research objective was to design, develop, and analyze different approaches to learning from similarities.

9. **Technical Contents and Accomplishments**

We made significant research accomplishments in a number of areas, some of which were planned, and some of which were outgrowths of the problems we were trying to solve. Specifically, this grant supported advances in quantifying contextual similarity [12], generative models for similarity-based classification [2][4][10][11], nearest-neighbor similarity-based learning [2], defining neighborhoods for local learning [3][6], Bayesian distribution-based estimation [1][5][7][9], and cost-sensitive multiclass classification [8]. We summarize each of these technical contributions separately in the next pages.

Quantifying Contextual Similarity

There are many methods to judge similarity between categorical feature vectors, but few take into account the context. In our work we incorporated the context of other given feature vectors by judging similarity as the conditional entropy given a Tversky framework [12].

Generative Models for Similarity-based Classification [2][4][10][11]

Similarity-based learning accepts as input a matrix of training similarities as well as a vector of similarities between the test sample and the training samples, and returns as output class labels.

An example is shown in the figure, where sample animals from three continents are shown, along with the network of similarities between them.

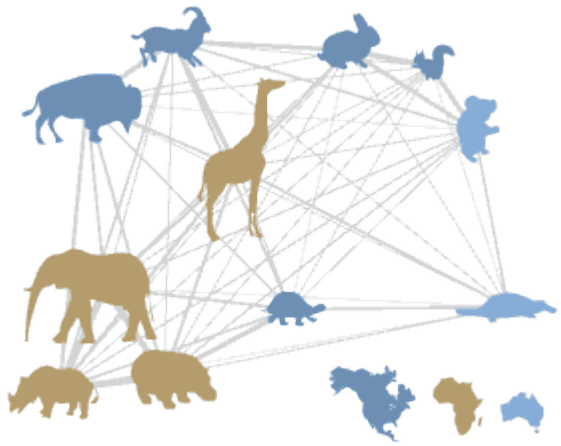

Generative classifiers have a model for each class-conditional distribution, and classify a test sample depending on which class-conditional model makes the test sample most likely. For standard metric learning, the most common class-conditional distribution is the Gaussian. We developed a generative model for the class-conditional probabilities of the test similarities, and showed that applying this model locally effectively reduces the model bias [2][4][10][11].

Nearest neighbor Similarity-based Learning [2]

The standard approach to weighting nearest neighbors is to relatively weight down neighbors that are less similar to the test sample. However, this does not account for redundancy between training samples. We showed that we could take into account both similarity and diversity by kernelizing our Euclidean-based work generalizing linear interpolation using a maximum entropy regularizer [17]. In the similarity-based learning architecture, this kernelizes to [2] minimizing the terms: $w^T S w - w^T s + k\, w^T w$, where w are the weights being solved for on the N neighboring training samples, S is the N x N similarity matrix between the N training samples, s is the N x 1 vector of similarities between the test sample and the N training samples, and *k* is a regularization parameter,

These kernel ridge interpolation weights achieved the statistically significantly best performance of all similarity-based classifiers on our largest, most statistically significant data set (Caltech 101), 25% better performance over just weighting nearest neighbors based on their similarity to the test sample [2], and were never statistically significantly worse than uniformly weighted k-nearest neighbors.

One of the problems encountered in similarity-based learning is that it is mathematically convenient to treat similarities as inner products in some space, so that the N x N matrix of the similarities between N samples is a positive definite matrix. However, in practice many similarities are not inner product functions, and sample similarity matrices are not positive definite. Examples are show in the figure below for three datasets. The Amazon dataset shows the similarity of 96 books to each other, where the similarity between book A and book B is measured as the number of people who buy book B after viewing book A. This similarity is not symmetric, and even violates the minimality principle. From the top plot of the similarity matrix,

one sees that the similarity matrix is very sparse – mostly books are not at all similar to each other. The bottom plot shows the eigenvalues for this similarity matrix. If all the eigenvalues are positive (that is, if all the eigenvalues were above the dotted line in the plot), then the similiarity matrix would be positive definite. But in fact some of the eigenvalues are negative. Similarly for Aural Sonar, which is a dataset where humans judged the similarity of different sonar signals, and the Protein dataset, which used a bioinformatics similarity.

For these cases that the similarity is not positive semidefinite, the corresponding classifiers must be solved for using global optimization. With global optimization it is difficult to know if you are not caught in a local minimum. The standard alternate is to approximate the similarity matrix with a positive semidefinite alternative. We analyzed and experimentally compared three methods to make this approximation: shifting, clipping, and flipping the eigenvalue spectrum [2]. Shifting means regularizing the similarity matrix by the identity matrix times the smallest eigenvalue, so that all the eigenvalues are shifted up such that the smallest eigenvalue is zero. Clipping means setting all negative eigenvalues to zero, which we showed is the optimal projection onto the cone of positive semidefinite matrices with respect to the Frobenius norm. Flipping means changing the sign of the negative eigenvalues to be positive; at face value this may seem odd, but we showed it produces eigenvalues that are the absolute values of the square root of the eigenvalues produced by replacing the similarity matrix S with S^TS. In addition, we showed that it is imperative that an appropriate modification also be applied to the test samples, or the classifier can perform very poorly.

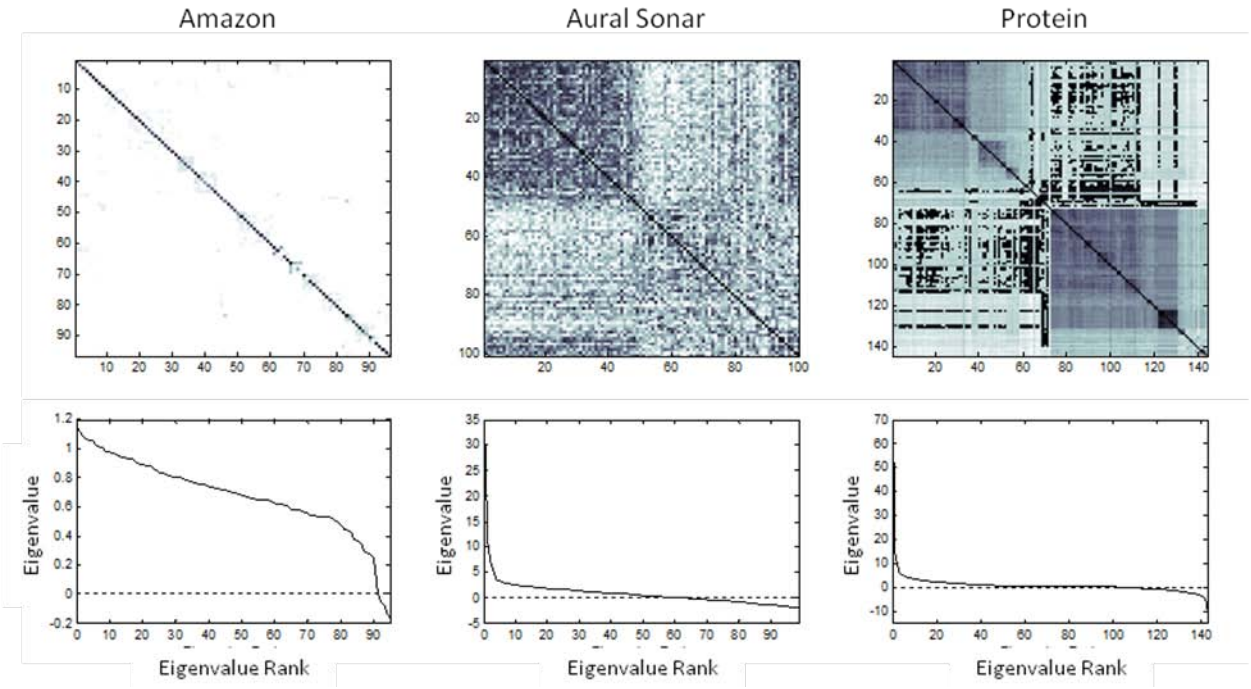

Defining Neighborhoods for Local Learning

Similarity-based learning often uses positive semidefinite approximations to indefinite similarity relationships, and these approximations are much less severe if calculated over a local neighborhood of a test sample. In fact, experimentally we saw that local similarity-based

classifiers always worked well [2]. This led us to study choosing optimal neighborhoods for local learning. In [6] we showed how to formalize the intuitive notion proposed by previous researchers that the neighborhood "should surround" the test sample. We formalized this by defining an "enclosing neighborhood" to be a neighborhood whose convex hull includes the test sample, and we proved that this results in minimum estimation variance when coupled with local linear regression. We also showed that this neighborhood size grows only linearly in the number of feature dimensions, and that it works significantly better than the state of the art in practice. We plan future work in kernelizing this work so that it can be applied to similarities.

Our other work in defining neighborhoods for local learning can be applied to any local classifier [3]. We called this method *completely lazy learning* because a neighborhood size does not have to be trained ahead of time, instead a number of neighborhood sizes are used and the discriminants averaged. This has a satisfying Bayesian interpretation, and yields excellent results.

Bayesian Distribution-based Estimation [1][5][7][9]:

This research led into some exciting discoveries in basic estimation theory. We generalized a recent result by Banerjee et al. [16] to the case of distributions and functions, showing that the expected function is the estimate that minimizes the expected Bregman divergence [5][9]. We used these results to make the quadratic discriminant analysis classifier more robust [7], and to form Bayesian estimates of differential entropy and relative entropy for any number of samples [1].

Cost-sensitive multi-class classification [8]:

Classifiers commonly output probabilities (e.g., Naive Bayes, k-NN, discriminant analysis) or discriminant functions (SVM's, neural nets), etc. For the two class case, the classifier usually decides whether it is class 1 or class 2 by testing whether the estimated probability $p(x) > ½$ or $p(x) < ½$. In the case of classifiers that output a discriminant function such as SVM's and neural nets, the classifier makes a decision based on whether the discriminant function $f(x)$ is > 0 or < 0. However, some classifiers tend to be biased up or down from this decision threshold. Friedman analyzed for the two-class case whether one could learn the threshold for a specific classifier, using an empirical risk minimization approach [13].

This problem can be even more serious in the multi-class case. The figure below illustrates a three-class classification problem – the triangle is the probability simplex, and the small triangles are the classifier's probability estimates for different test samples, a triangle close to the left-bottom corner labeled "3" means the probability of class 3 is high. A triangle in the middle of the simplex would represent a probability estimate that was uniform over the three classes. The dotted lines show the decision boundaries a standard classifier would apply to the probability simplex in order to classify the estimates. The left simplex shows examples from a naïve Bayes classifier. The right simplex shows examples from a k-NN classifier. Each small triangle (probability estimate) is linked to a circle that denotes the corresponding correct probability. One sees that the naïve Bayes' classifier is biased towards undersmoothing its probability estimates towards the uniform distribution over classes, while the k-NN classifier is biased towards oversmoothing its estimates towards the uniform distribution.

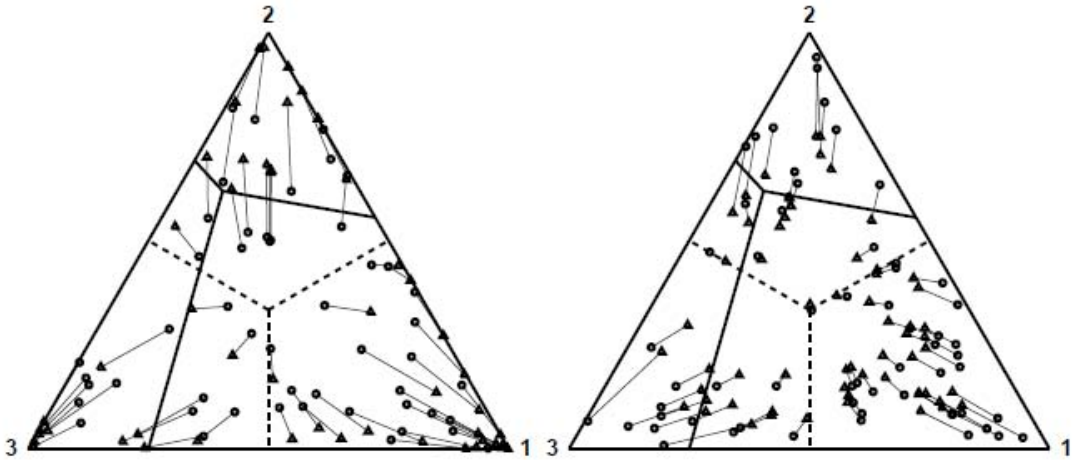

(a) Naive Bayes example (b) k-NN example

Our work in this area [8] considered learning the probability-thresholds for multiple classes using an empirical risk minimization strategy with a parameterized class of decision boundaries over the simplex. We showed experimental and theoretical advantages compared with previous approaches by Domingos [14] and La Flache [15].

Final Report for ONR CODE 30 CIED 6.1 Basic Research Effort

10. **Deliverables, Personnel, Awards, Publications, Presentations, and Patents**

Deliverable	Date
Final Technical Report (this report) with SF298	**January 2011**

Table 1. Deliverables

Final Report for ONR CODE 30 CIED 6.1 Basic Research Effort

	Total #	Name	Organization
PIs	1	Maya Gupta	**University of Washington**
Co-PIs	1	John Miyamoto	**University of Washington**
Grad Students	6	Santosh Srivastava	**University of Washington**
		Luca Cazzanti	**University of Washington**
		Eric Garcia	**University of Washington**
		Yihua (James) Chen	**University of Washington**
		Sergey Feldman	**University of Washington**
		Alex Marin	**University of Washington**

Table 2. Personnel Information

	Name	Awards (Year Received)	Prize (Year Received)	Recognition (Year Received)
PIs	Maya Gupta	PECASE 2007, ONR YIP 2007		**Univ. of Washington Dept. of Electrical Engineering Distinguished Teaching Award**
Grad Students	Luca Cazzanti			**Chosen to be 1 of 2 American interns at NATO NURC in 2006**
	Sergey Feldman	UW EE Innovator Fellowship 2007		
	Eric Garcia	Intel GEM Fellowship 2005-2007		

Table 3. Awards/Prizes/Recognitions

Final Report for ONR CODE 30 CIED 6.1 Basic Research Effort

Name	Publication (Date)	Conference Presentation (Date)	Patent (Date)
Luca Cazzanti and Maya R. Gupta		Information-theoretic and set-theoretic similarity, *Proc. Intl. Symposium Information Theory* (2006).	
Maya R. Gupta, Luca Cazzanti, and Anjali Koppal		Maximum Entropy Generative Models for Similarity-based Learning, *Proc. of the IEEE Intl. Symposium on Information Theory* (2007).	
Santosh Srivastava, Maya R. Gupta, and Bela Frigyik	Bayesian Quadratic Discriminant Analysis, *Journal of Machine Learning Research*, vol. 8, pp. 1277-1305 (2007).		
Luca Cazzanti and Maya R. Gupta		Local Similarity Discriminant Analysis, *Intl. Conf. Machine Learning (ICML)* (2007).	
Maya R. Gupta, Luca Cazzanti, and Anjali J. Koppal	Generative Models for Similarity-based Classification, *Pattern Recognition*, vol. 41, no. 7, pp. 2289-2297 (2008).		
Maya R. Gupta, Eric Garcia, and Erika Chin	Adaptive Local Linear Regression with Application to Printer Color Management, *IEEE Trans. on Image Processing*, vol. 17, no. 6, 936-945 (2008).		

Bela Frigyik, Santosh Srivastava, and Maya R. Gupta		Functional Bregman Divergence, *Proc. IEEE Intl. Symp. on Information Theory* (2008).	
Deirdre B. O'Brien, Maya R. Gupta and Robert M. Gray		Cost-sensitive multi-class classification from probability estimates, *Intl. Conf. Machine Learning (ICML)* (2008).	
Bela Frigyik, Santosh Srivastava, and Maya R. Gupta.	Functional Bregman Divergence and Bayesian Estimation of Distributions, *IEEE Trans. on Information Theory*, vol. 54, no. 11, 5130-5139 (2008).		
Eric Garcia, Sergey Feldman, Maya R. Gupta, and S. Srivastava	Completely Lazy Learning. *IEEE Trans. on Knowledge and Data Engineering* (2009).		
Yihua Chen, Eric Garcia, Maya R. Gupta, Luca Cazzanti, and Ali Rahimi.	Similarity-based Classification: Concepts and Algorithms, *Journal of Machine Learning Research*, vol. 10, 747-776, 2009.		
Maya R. Gupta and S.antosh Srivastava.	Parametric Bayesian Estimation of Differential Entropy and Relative Entropy, To appear in *Entropy (20 pages)* (2010).		

Table 4. Publications, Conference Presentations and Patents

11. **References:** (In support of Sections 7-9 above.)

1. Parametric Bayesian Estimation of Differential Entropy and Relative Entropy," M. R. Gupta and S. Srivastava. To appear in *Entropy (20 pages), 2010*.

2. "Similarity-based Classification: Concepts and Algorithms," Yihua Chen, Eric Garcia, Maya R. Gupta, Luca Cazzanti, and Ali Rahimi. Journal of Machine Learning Research, vol. 10, pg. 747-776, 2009.

3. "Completely Lazy Learning," Eric Garcia, Sergey Feldman, Maya R. Gupta, and S. Srivastava. IEEE Trans. on Knowledge and Data Engineering, 2009.

4. "Generative Models for Similarity-based Classification," Maya R. Gupta, Luca Cazzanti, and Anjali J. Koppal. Pattern Recognition, vol. 41, no. 7, pp. 2289-2297, 2008.

5. "Functional Bregman Divergence and Bayesian Estimation of Distributions," Bela Frigyik, Santosh Srivastava, and Maya R. Gupta. IEEE Trans. on Information Theory vol. 54, no. 11, 5130-5139, 2008.

6. "Adaptive Neighborhoods for Local Linear Regression," Maya R. Gupta, Eric Garcia, and Erika Chin. IEEE Trans. on Image Processing, vol. 17, no. 6, 936-945, 2008.

7. "Bayesian Quadratic Discriminant Analysis," Santosh Srivastava, Maya R. Gupta, and Bela Frigyik. Journal of Machine Learning Research, vol. 8, pp. 1277-1305, 2007.

8. "Cost-sensitive multi-class classification from probability estimates," D. B. OBrien and M. R. Gupta and R. M. Gray, Intl. Conf. Machine Learning (ICML), 2008.

9. "Functional Bregman Divergence," Bela Frigyik, Santosh Srivastaa, and Maya R. Gupta, Proc. IEEE Intl. Symp. on Information Theory, 2008.

10. "Local Similarity Discriminant Analysis," Luca Cazzanti and Maya R. Gupta, Intl. Conf. Machine Learning (ICML), 2007.

11. "Maximum Entropy Generative Models for Similarity-based Learning," Maya R. Gupta, Luca Cazzanti and Anjali Koppal, Proc. of the IEEE Intl. Symposium on Information Theory, 2007.

12. "Information-theoretic and set-theoretic similarity," Luca Cazzanti and Maya R. Gupta, Proc. of the IEEE Intl. Symposium on Information Theory, 2006.

13. "On bias, variance, 0/1-loss,and the curse-of-dimensionality. J. H. Friedman, Data Mining and Knowledge Discovery, 1, 55-77, 1997.

14. "Metacost: A general method for making classifiers cost-sensitive." P. Domingos. Proc. of 5th International Conference on Knowledge Discovery and Data Mining (pp. 155- 164) 1999.

15. "Improving accuracy and cost of two-class and multi-class probabilistic classifiers using ROC curves." N. Lachice and P. Flach. Proc. of 20th International Conference on Machine Learning (pp. 416-423). 2003.

16. “Clustering with Bregman divergences,” A. Banerjee, S. Merugu, I. S. Dhillon, and J. Ghosh, Journal of Machine Learning Research. Vol. 6, pp. 1705-1749, 2005.

17. “Nonparametric supervised learning by linear interpolation with maximum entropy,” Maya R. Gupta, Robert M. Gray, and Richard A. Olshen. IEEE Trans. on Pattern Analysis and Machine Intelligence, vol. 28, no. 5, pp. 766-781, 2006.

Final Report for ONR CODE 30 CIED 6.1 Basic Research Effort

1. **"Detection and modeling of IEDs camouflaged by obscuring layers"**
2. **Prime Offeror:** University of Washington, Seattle, WA, USA
3. **Subcontractors:** N/A
4. **Period of Performance: August 1, 2005 to December 31, 2009**
5. **Submitted by:** Yasuo Kuga, ykuga@u.washington.edu, 206-543-0478
6. **Business Contact:** Noel Henry, henry@u.washington.edu, 206-685-1979

7. **Background/Scope of Effort**

The detection and imaging of IEDs in obscured and complex environments is vital for the on-going efforts to combat explosive device deployment. We focused our effort on understanding the effects of random, obscured environments on the imaging and detection of objects and the methods that will enhance the imaging and detection using electromagnetic waves ranging from millimeter waves to optical waves. We investigated several methods to improve imaging and detection of objects. We started from the detection and imaging of objects obscured by clothing, which was intended for detection of an explosive on a person. Then, we focused on detection and imaging of an object in the presence of clutter that was aimed at road-side explosives using several imaging methods, including acoustic-induced vibration detection using millimeter wave (MMW) radar. Furthermore, we investigated the detection of a thin, long wire that may be used as a command wire.

8. **Summary/Abstract**

The goal of our research project was to improve the science behind electromagnetic wave imaging and detection of a suspicious object, such as an improvised explosive device (IED), in obscuring, random, and complex media. Our research can be categorized into three parts according to the application in IED detection in the theater. First, we focused on detection and imaging of objects underneath clothing, intended for detection of a hidden IED underneath clothing on a person. Second, we investigated methods to detect and image an object in the presence of surrounding clutter. This effort has applications to the detection of hidden road-side explosives. Finally, we concentrated on detecting and imaging a small thin wire. This offers another way to detect an explosive that has been connected to a trigger through a command wire. In each part, we combined several techniques for modeling, detecting, and imaging of electromagnetic waves at several frequencies (millimeter wave, terahertz wave, infrared, and optical wave); these techniques include include space-time-frequency correlation of waves and signal processing.

9. **Technical Contents and Accomplishments**

(1) Detection of a hidden IED underneath clothing

To detect and image a hidden IED underneath clothing, we exploit the behavior of wave scattering at MMW and terahertz (THz) frequencies. Detection and imaging of a hidden object at MMW and THz frequencies offers several advantages, such as being non-intrusive and non-ionizing. However, it is well-known that, in electromagnetic imaging, there is a trade-off between image resolution and the penetration depth. MMW and THz frequencies seem to offer a balance in the trade-off, while lower frequency ranges (microwave and lower frequencies) offer unacceptable resolution at a stand-off distance, and higher frequency ranges (optical) cannot penetrate through obscuring layers.

We started by gathering information about the material properties (most importantly, the dielectric constant) at MMW and THz frequencies. Then, we constructed a model for wave propagation through multilayer media with rough surface interfaces. Active radar imaging based on the reflection of waves from multilayer media is then used to detect and construct images showing potential suspicious objects. We have also constructed a model to simulate passive

imaging. Active and passive imaging can be used together because active imaging will reveal the shape and size of a concealed dielectric object, while passive imaging can differentiate objects of different emissivity (useful for detection of metal). The results have been presented in [11, 13] and are shown in Fig. 1.

We also applied an angular correlation function for detection of the presence of particle scattering. This is based on the assumption that an IED on a person usually contains shrapnel. The phase information of the angular correlation has been analyzed and shown to be useful for detection of the presence of particle scattering. This technique can be used in conjunction with the previous active and passive imaging to identify the presence of particles in a suspicious volume.

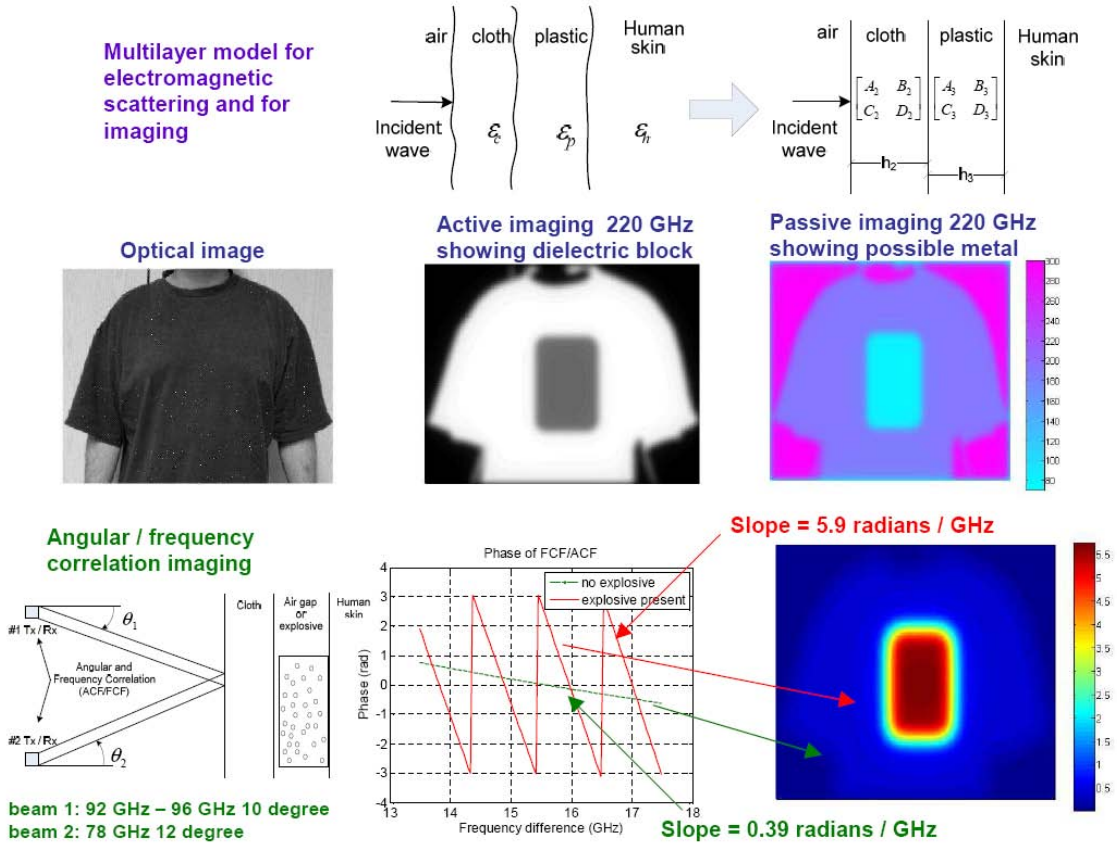

Fig 1: Multilayer modeling of electromagnetic scattering, MMW imaging simulations, and the angular/frequency correlation imaging for detection and imaging of an object underneath clothing.

(2) Detection of an object obscured by random complex media or surrounded by clutter

We investigated the generalized space-time-frequency formulation for wave propagation and scattering in random scattering media and its application for target detection. We formulated a two-frequency mutual coherence function that gives the correlation of waves with two different frequencies in the presence of multiple scattering media. The detailed formulation is reported in [7, 9, 10, 12]. We applied this formulation to the imaging of an object based on a scanned focused beam and showed effects that random scattering media have on imaging in terms of resolution (Fig. 2).

We also investigated super-resolution imaging using the time-reversal imaging method. Time-reversal imaging shows a surprising result that the image resolution improves in the presence of a random scattering medium. We showed analytically the super-resolution effects,

and we numerically verified the results using the Finite-Difference Time-Domain method[2, 3, 4, 5, 14] (Fig. 3).

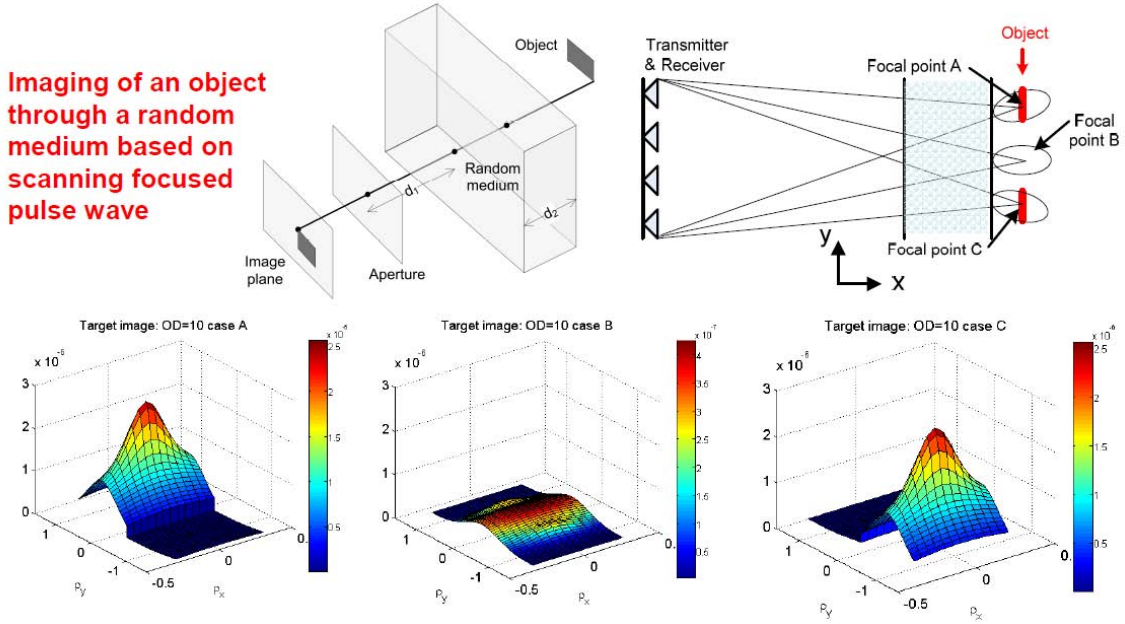

Fig 2: Imaging of objects through random scattering media using a focused pulse wave.

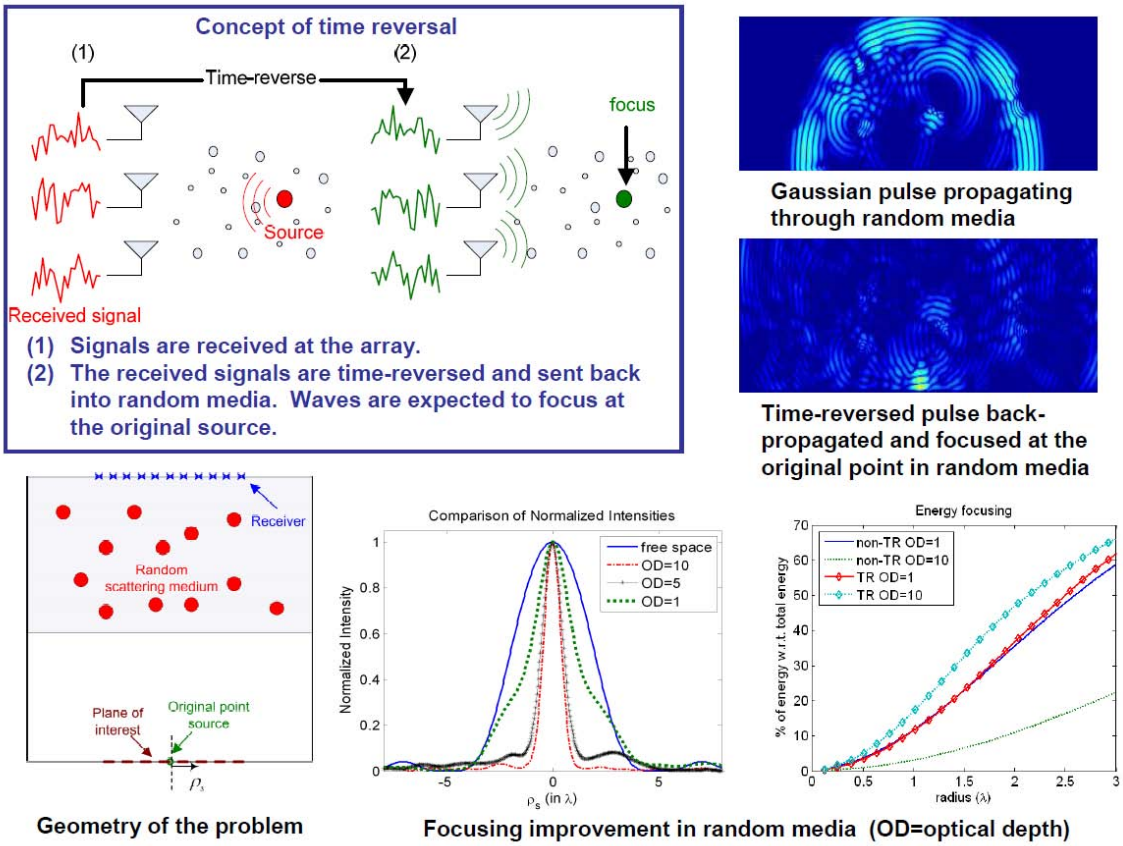

Fig 3: Super-resolution based on the time-reversal method.

We also investigated a radar imaging method based on Doppler information from acoustic-induced vibration. In electromagnetic imaging, we rely on the contrast in electromagnetic response (dielectric constant). However, Doppler imaging based on acoustic-induced vibration relies on the contrast in the density of bulk material. This offers another dimension for detecting a suspicious object among clutter. The concept and results of this method are reported in [8] and shown in Fig. 4.

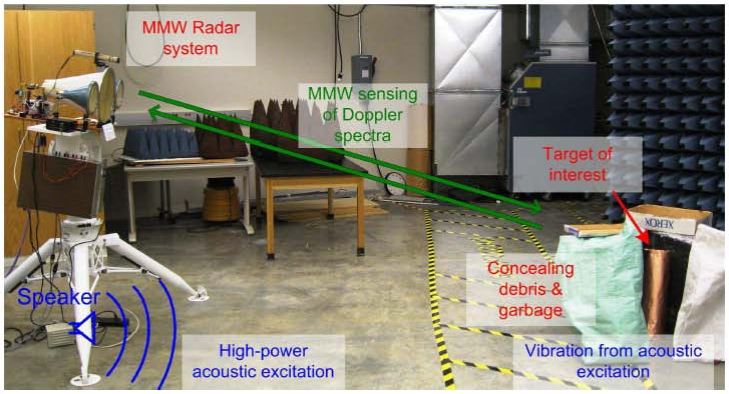

CONCEPT

- **Acoustic wave excitation creates vibration of an object and its surroundings. Their mechanical responses depend on materials and structures.**
- **MMW radar detects the vibration characteristics using Doppler spectra.**

Doppler images using 2-D scan and short pulse
with a known vibrating source at 20 Hz (discrimination of an active source)

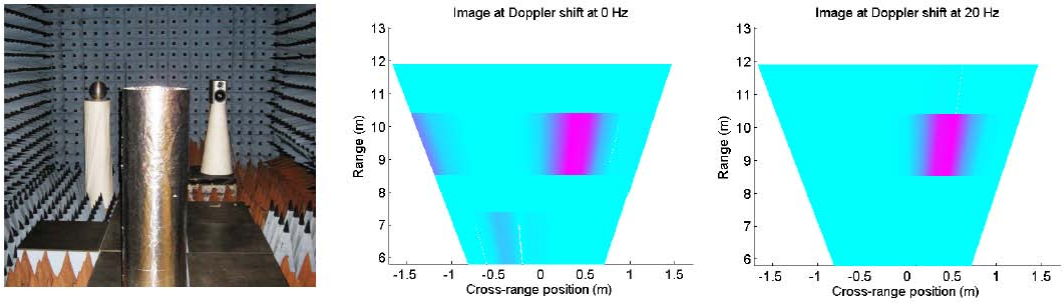

Fig 4: Radar Doppler imaging of targets in clutter based on acoustically-induced vibration.

(3) Detection of a thin wire

IEDs are commonly triggered manually using a command wire. Therefore, methods to detect a thin long wire can be very useful in the detection of many concealed explosives. We investigated two, independent methods to detect a long, thin wire. We primarily focused on passive detection methods because they offer covertness and require less power.

First, we exploited the polarization and scattering nature of a long, thin wire. The scattering cross sections of the wire for different polarizations can offer clues on the presence of a wire and its orientation. The cross sections of a long wire were analyzed and compared with the expected scattering from a rough ground surface. Second, we investigated polarimetric infrared imaging. We exploited the difference in emission of a smooth, man-made object (a long wire, in this case) and rough natural terrain. The concept and results of both passive methods are illustrated in Fig. 5.

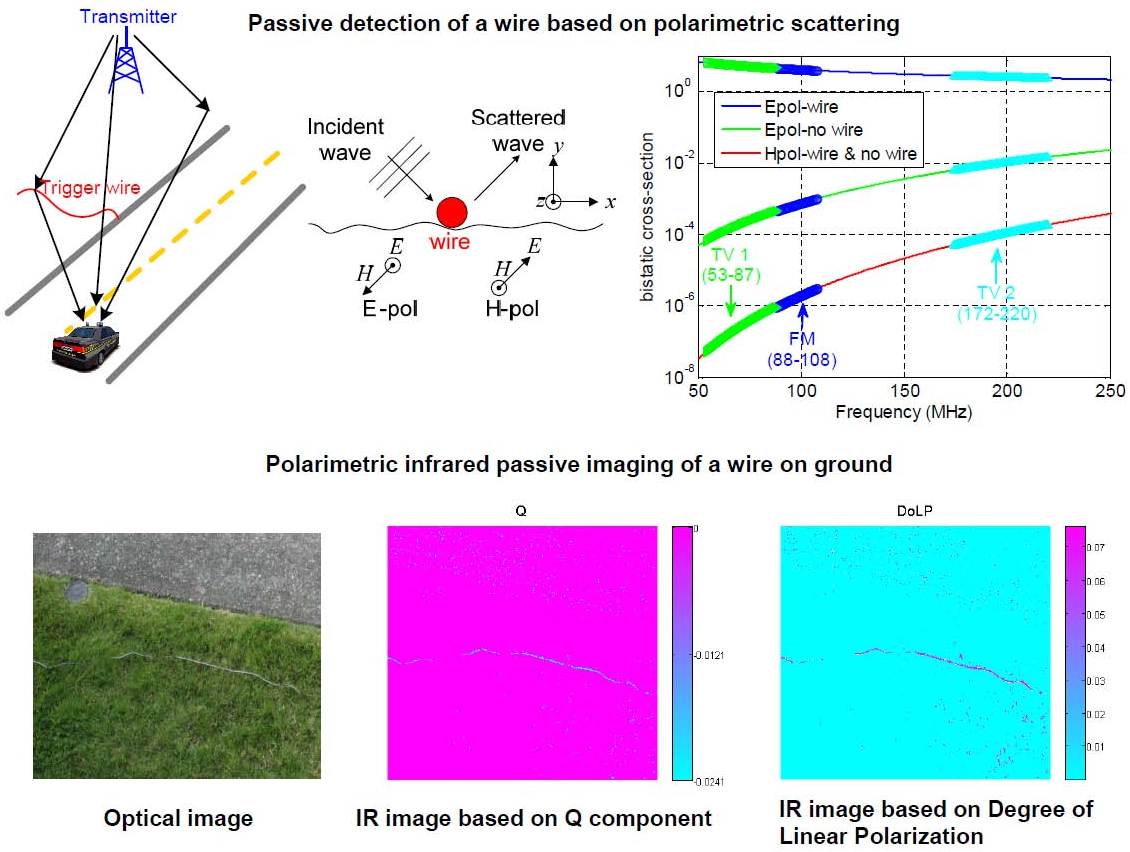

Fig 5: Passive detection methods for a long, thin wire in the presence of background scattering.

Final Report for ONR CODE 30 CIED 6.1 Basic Research Effort

10. **Deliverables, Personnel, Awards, Publications, Presentations, and Patents**

Deliverable	Date
Final Technical Report (this report)	**January 2011**

Table 1. Deliverables

Final Report for ONR CODE 30 CIED 6.1 Basic Research Effort

	Total #	Name	Organization
PIs	1	Yasuo Kuga	**University of Washington**
Co-PI	1	Akira Ishimaru	**University of Washington**
Grad Students	3	Jun-ho Cha	**University of Washington**
		Colin Reinhardz	**University of Washington**
		Thomas Chan	**University of Washington**
Post Doc	1	Sermsak Jaruwatanadilok	**University of Washington**

Table 2. Personnel Information

	Name	Award (Year Received)	Prize (Year Received)	Recognition (Year Received)
PIs	Yasuo Kuga	*NASA Tech Brief Award, 2006*		
Co-PIs	Akira Ishimaru	*NASA Tech Brief Award, 2006*		
Grad Students	Colin Reinhardz	SMART Fellowship 2006-2009		
Post Docs	Sermsak Jaruwatanadilok	*NASA Tech Brief Award, 2006*		
Research Assistants	N/A			

Table 3. Awards/Prizes/Recognitions

Final Report for ONR CODE 30 CIED 6.1 Basic Research Effort

Name	Publication (Date)	Conference Presentation (Date)	Patent (Date)
S. Jaruwatanadilok and A. Ishimaru	"Electromagnetic coherent tomography array imaging in random scattering media," *IEEE Antennas and Wireless Propagation Letters*, vol. 7, pp. 524-27, 2008.		
T. Chan, S. Jaruwatanadilok, Y. Kuga, and A. Ishimaru	"Numerical study of the time reversal effects in a random scattering media on super-resolution and comparison with analytical model," *Waves in Random and Complex Media*, vol. 19, no.4, pp. 627-39, 2008.		
T. Chan, S. Jaruwatanadilok, Y. Kuga, and A. Ishimaru		"Investigation of super-resolution in a random scattering media using numerical FDTD time-reversal simulations and beamforming processing techniques," *URSI-APS*, San Diego, CA, USA, June 2008.	
T. Chan, S. Jaruwatanadilok, Y. Kuga, and A. Ishimaru		"Investigation of time reversal effects in random scattering media on super-resolution by FDTD Monte Carlo simulations," *URSI Meeting*, Boulder, CO, USA, January 2008.	

A. Ishimaru, S. Jaruwatanadilok, Y. Kuga	"Time reversal effects in random scattering media on superresolution, shower curtain effects, and backscattering enhancement," *Radio Science,* vol. 42, pp. RS6S28, 2007.		
A. Ishimaru, S. Jaruwatanadilok, and Y. Kuga	"Imaging of a target through random media using a short-pulse focused beam," *IEEE Transactions on Antennas and Propagation*, vol. 55, no. 6, pp. 1622-1629, 2007.		
A. Ishimaru, S. Jaruwatanadilok, and Y. Kuga		"Imaging of objects through scattering random medium layers using a pulsed scanning focused beam," *EMTS*, Ottawa, Canada, July 2007.	
S. Jaruwatanadilok, T. Chan, Y. Kuga, and A. Ishimaru		"Detection of an object in a cluttered environment using acoustic-induced Doppler spectrum feature from an active millimeter wave radar system," *URSI-APS*, Ottawa, Canada, July 2007.	
A. Ishimaru, S. Jaruwatanadilok, and Y. Kuga	"Short pulse detection and imaging of objects behind obscuring random layers," *Waves in Random and Complex Media*, vol. 16, no. 4, pp. 509-20, 2006.		
Y. Kuga, A. Ishimaru, and S. Jaruwatanadilok		"Short pulse detection of objects behind obscuring random layers," *IGARSS*, Denver, CO, July 31-August 4, 2006.	

S. Jaruwatanadilok, Y. Kuga, and A. Ishimaru		"An electromagnetic model for plastic composite materials under obscuring layers," *URSI-APS*, Albuquerque, NM, July 9-14, 2006.	
A. Ishimaru, S. Jaruwatanadilok, and Y. Kuga		"Imaging and detection of hidden objects behind obscuring random media," *URSI-APS*, Albuquerque, NM, July 9-14, 2006.	
S. Jaruwatanadilok, Y. Kuga, A. Ishimaru, and E. Thorsos		"An electromagnetic model for detecting explosives under obscuring layers," *International Symposium on Technology and the Mine Problem*, Monterey, CA, May 2-4, 2006.	
A. Ishimaru, S. Jaruwatanadilok, and Y. Kuga		"Time-reversal techniques applied to communications through unknown obscuring medium," *AMS SIAM*, San Antonio, TX, January 10-15, 2006.	

Table 4. Publications, Conference Presentations and Patents

11. **References:** (In support of Sections 7-9 above.)

1. S. Jaruwatanadilok and A. Ishimaru, "Electromagnetic coherent tomography array imaging in random scattering media," *IEEE Antennas and Wireless Propagation Letters*, vol. 7, pp. 524-27, 2008.
2. T. Chan, S. Jaruwatanadilok, Y. Kuga, and A. Ishimaru, "Numerical study of the time reversal effects in a random scattering media on super-resolution and comparison with analytical model," *Waves in Random and Complex Media*, vol. 19, no. 4, pp. 627-39, 2008.
3. T. Chan, S. Jaruwatanadilok, Y. Kuga, and A. Ishimaru, "Investigation of super-resolution in a random scattering media using numerical FDTD time-reversal simulations and beamforming processing techniques," *URSI-APS*, San Diego, CA, USA, June 2008.
4. T. Chan, S. Jaruwatanadilok, Y. Kuga, and A. Ishimaru, "Investigation of time reversal effects in random scattering media on super-resolution by FDTD Monte Carlo simulations," *URSI Meeting*, Boulder, CO, USA, January 2008.
5. A. Ishimaru, S. Jaruwatanadilok, and Y. Kuga, "Time reversal effects in random scattering media on superresolution, shower curtain effects, and backscattering enhancement," *Radio Science*, vol. 42, pp. RS6S28, 2007.
6. A. Ishimaru, S. Jaruwatanadilok, and Y. Kuga, "Imaging of a target through random media using a short-pulse focused beam," *IEEE Transactions on Antennas and Propagation*, vol. 55, no. 6, pp. 1622-1629, 2007.
7. A. Ishimaru, S. Jaruwatanadilok, and Y. Kuga, "Imaging of objects through scattering random medium layers using a pulsed scanning focused beam," *EMTS*, Ottawa, Canada, July 2007.
8. S. Jaruwatanadilok, T. Chan, Y. Kuga, and A. Ishimaru, "Detection of an object in a cluttered environment using acoustic-induced Doppler spectrum feature from an active millimeter wave radar system," *URSI-APS*, Ottawa, Canada, July 2007.
9. A. Ishimaru, S. Jaruwatanadilok, and Y. Kuga, "Short pulse detection and imaging of objects behind obscuring random layers," *Waves in Random and Complex Media*, vol. 16, no. 4, pp. 509-20, 2006.
10. Y. Kuga, A. Ishimaru, and S. Jaruwatanadilok, "Short pulse detection of objects behind obscuring random layers," *IGARSS*, Denver, CO, July 31-August 4, 2006.
11. S. Jaruwatanadilok, Y. Kuga, and A. Ishimaru, "An electromagnetic model for plastic composite materials under obscuring layers," *URSI-APS*, Albuquerque, NM, July 9-14, 2006.
12. A. Ishimaru, S. Jaruwatanadilok, and Y. Kuga, "Imaging and detection of hidden objects behind obscuring random media," *URSI-APS*, Albuquerque, NM, July 9-14, 2006.
13. S. Jaruwatanadilok, Y. Kuga, A. Ishimaru, and E. Thorsos, "An electromagnetic model for detecting explosives under obscuring layers," *International Symposium on Technology and the Mine Problem*, Monterey, CA, May 2-4, 2006.
14. A. Ishimaru, S. Jaruwatanadilok, and Y. Kuga, "Time-reversal techniques applied to communications through unknown obscuring medium," *AMS SIAM*, San Antonio, TX, January 10-15, 2006.

Final Report for ONR CODE 30 CIED 6.1 Basic Research Effort

1. **"Change Point Detection in Multivariate Data Streams"**
2. **Prime Offeror:** University of Washington
3. **Subcontractors:** None
4. **Period of Performance:** 1 August 2005 to 31 December 2009
5. **Submitted by:** Caren Marzban, marzban@u.washington.edu, 206-616-8709
6. **Business Contact:** Monty Bolstad, monty@apl.washington.edu, 206-543-9826

7. **Background/Scope of Effort:** The problem of detecting when a change has occurred can be cast into the problem of detecting an IED threat. Most existing methods for change detection examine a single stream of data. Also, most methods assume the data to be independent and identically distributed. Moreover, there exists little in terms of mathematical tools for properly assessing the performance of a change detection algorithm. These limitations prompted us to develop a change detection framework wherein each of these constraints is addressed. We also extended the framework to one where the change detector can be tailored to meet the needs of a specialized user/agent.

8. **Summary/Abstract:** Under the assumption that an IED threat can be identified by a careful examination of multiple data streams, we considered the problem of detection when a change has occurred in the relationships between variables in such streams. We began by studying how best to detect changes in multivariate data streams for which the streamed data are independent of one another at different times. We studied how the false alarm rate can be properly calibrated. We also developed a revised version of the Receiver's Operating Characteristic (ROC) curve suited to change detection problems. We also explored the possibility of using supervised learning as a means of detecting changes between variables in data streams. We addressed the problems that arise when the streamed data are not independent samples, but rather are samples from a correlated multivariate time series. Finally, we considered extensions in which the data streams involve images collected over time.

9. **Technical Contents and Accomplishments:** In the first phase of the project we considered the problem of detecting changes in a multivariate data stream in an unsupervised fashion. In other words, we allowed for change to occur not necessarily in any single stream, but also in the relationship between streams. The reference to "unsupervised" means that the type of change is not specified by a user/agent. In this context, a change detector is defined by a detection algorithm and an alarm threshold. A detection algorithm maps the stream of input vectors into a univariate detection stream. The detector signals a change when the detection stream exceeds the chosen alarm threshold. We consider two aspects of the problem: (1) setting the alarm threshold and (2) measuring and comparing the performance of detection algorithms. We assume for training we are given a segment of the stream where changes of interest are marked. We present evidence that, without such marked training data, it might not be possible to accurately estimate the false alarm rate for a given alarm threshold. Commonly used approaches assume the data stream consists of independent observations, an implausible assumption given the time series nature of the data. Lack of independence can lead to estimates that are badly biased. Marked training data can also be used for realistic comparison of detection algorithms. We define a version of the receiver operating characteristic curve adapted to the change detection problem and propose a block bootstrap for comparing such curves. We illustrate the proposed methodology using multivariate data derived from an image stream. A technical report (Kim et al. 2009b), a conference presentation (Stuetzle et al. 2008), and a journal article (Kim et al. 2009a) were produced from this work. A website describing the project was also produced (Kim 2008).

The aforementioned approach to change detection did not require labeled data (i.e., data where changes of interest have been labeled by a user/agent). Such data were required only for properly assessing the performance of the detection algorithm. In the second phase of the project, we developed a "targeted" (or supervised) method, wherein labeled data are required for the development of the change detector. This method assures that information regarding changes of interest to a user/agent is injected into the change detector.

Figure 1 compares and contrasts the two approaches. A general change detection scheme begins by being exposed to some data stream. The detection algorithm then produces a univariate detection stream, which in turn is thresholded in order to convert the stream to a binary action of raising or not raising an alarm. In a nontargeted approach, what we call the detection algorithm consists of some 2-sample statistic. Some statistics (e.g., Student's t) are sensitive to changes in the mean of the stream. Others (e.g., Szekely) have power against all alternatives. As such, the choice of the statistic is related to the type of change the detection algorithm can detect. However, if the type of change of interest is encoded in existing data, then one can employ the more direct targeted approach. Here, the detection algorithm consists of a classifier that has been trained on labeled data, with the labels denoting events of interest and uninteresting events. Such a classifier produces a stream we call the score stream. Some classifiers produce the probability that an event can occur, in which case the score stream is a stream of probabilities. Other classifiers may not produce such probabilities. However, all classifiers will produce a score stream such that higher values of the stream can be associated with the existence of an event. Effectively, then, the classifier maps a multivariate stream to a univariate stream in such a way that the existence of any type of change in the former will be associated with a level change in the latter.

In the targeted approach we consider the problem of event detection based upon a multivariate data stream characterizing some system. Most of the time the system is quiescent -- nothing of interest is happening -- but occasionally events of interest occur. The goal of event detection is to raise an alarm as soon as possible after the onset of an event. A simple way of addressing the event detection problem is to look for changes in the data stream and equate "change" with "onset of event." However, there might be many kinds of changes in the stream that are uninteresting. We assume that we are given a segment of the stream where interesting events have been marked. We developed a method for using these training data to construct a targeted detector that is specifically sensitive to changes signaling the onset of interesting events.

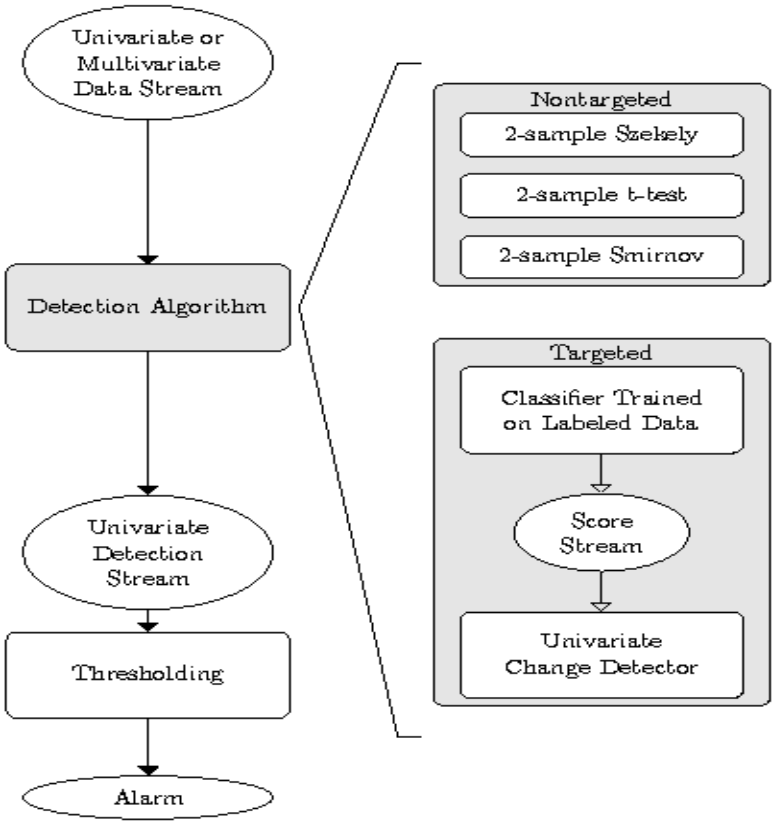

Figure 1. Comparing a targeted event detection scheme (left) with an untargeted (or unsupervised) scheme (right).

In the process of developing the above-mentioned techniques, we examined a well-known motion detection method called Optical Flow. Although we discovered that the optical flow method does not immediately address the problem we were tackling, we found out that it does solve another problem, namely that of assessing the quality of a forecast field in meteorological problems. As a result, a paper has been produced reporting the findings (Marzban and Sandgathe, 2010).

Final Report for ONR CODE 30 CIED 6.1 Basic Research Effort

10. **Deliverables, Personnel, Awards, Publications, Presentations, and Patents**

Deliverable	Date
Final Technical Report (this report)	**January 2011**

Table 1. Deliverables

Final Report for ONR CODE 30 CIED 6.1 Basic Research Effort

	Total #	Name	Organization
PIs	1	Werner Stuetzle	**Univ. of Washington/Dept. of Statistics**
Co-PIs	2	Donald Percival	**Univ. of Washington/APL**
		Caren Marzban	**Univ. of Washington/Dept. of Statistics**
Grad Students	1	Albert Kim	**Univ. of Washington/Dept. of Statistics**
Post Docs	0		
Research Assistants	0		

Table 2. Personnel Information

	Name	Award (Year Received)	Prize (Year Received)	Recognition (Year Received)
PIs	Werner Stuetzle			**Appointed Division Dean, College of Arts and Sciences, University of Washington (2006)**
Co-PIs	Donald Percival			**Appointed Professor WOT, Department of Statistics, University of Washington (2008)**

Table 3. Awards/Prizes/Recognitions

Final Report for ONR CODE 30 CIED 6.1 Basic Research Effort

Name	Publication (Date)	Conference Presentation (Date)	Patent (Date)
Albert Kim	"Using Labeled Data to Evaluate Change Detectors in a Multivariate Streaming Environment," A. Y. Kim, C. Marzban, D. B. Percival, and W. Stuetzle, *Signal Processing, 89* (2009), pp. 2529–2536.	"Using Labeled Data to Evaluate Change Detectors in a Multivariate Streaming Environment," W. Stuetzle, D. B. Percival, C. Marzban, and A. Y. Kim, Activity number 22, *2008 Joint Statistical Meetings, Denver. CO*, August 3–17.	
Werner Stuetzle	"Targeted Change Detection," W. Stuetzle, D. B. Percival, and C. Marzban, submitted to *Signal Processing* (2010).		
Caren Marzban	"Optical Flow for Verification," C. Marzban and S. Sandgathe. conditionally accepted at *Weather and Forecasting* (2010).		

Table 4. Publications, Conference Presentations and Patents

Final Report for ONR CODE 30 CIED 6.1 Basic Research Effort

11. **References:** (In support of Sections 7-9 above.)

Stuetzle, W., D. B. Percival, C. Marzban, and A. Y. Kim (2008): "Using Labeled Data to Evaluate Change Detectors in a Multivariate Streaming Environment," Activity number 22, *2008 Joint Statistical Meetings, Denver. CO,* August 3-17.

Kim, A. Y., C. Marzban, D. B. Percival, and W. Stuetzle (2009a): "Using Labeled Data to Evaluate Change Detectors in a Multivariate Streaming Environment," *Signal Processing, 89*(12), 2529-2536; doi:10.1016/j.sigpro.2009.04.011.

Kim, A. Y., C. Marzban, D. B. Percival, and W. Stuetzle (2009b): "Using Labeled Data to Evaluate Change Detectors in a Multivariate Streaming Environment," Technical Report no. 534, University of Washington Department of Statistics.

Stuetzle, W., D. Percival, and C. Marzban (2010): "Targeted Event Detection," submitted to *Signal Processing*.

Marzban, C. and S. Sandgathe (2010): "Optical Flow for Verification," conditionally accepted at *Weather and Forecasting*.

Kim, A. Y. (2008): A website containing labeled data used for the evaluation of the untargeted change detector; http://www.stat.washington.edu/research/changedetection/.

Final Report for ONR CODE 30 CIED 6.1 Basic Research Effort

1. **"Terahertz scattering for detection of Improvised Explosive and Bio-Agent Dispersal Devices"**
2. **Prime Offeror:** University of Washington
3. **Subcontractors:** Portland State University
4. **Period of Performance:** August 1, 2005 – December 31, 2009
5. **Submitted by:** Dale P. Winebrenner, dpw@apl.washington.edu, 206.543.1393
6. **Business Contacts:** Monty Bolstad, 206.543.9826, monty@apl.washington.edu; Bill Helsley, 503.725.3417, helsleyw@pdx.edu
7. **Background/Scope of Effort**: The physics of interaction between key materials and electromagnetic radiation at so-called terahertz (THz) frequencies of 10^{12} to 10^{13} Hz has been considered promising, on two counts, for the detection of concealed explosives. First, characteristic absorption features in reflection spectra of explosives may provide a basis for discrimination from other materials. Second, common obscuring materials (e.g., cellulose, plastic) are translucent to THz radiation, so detection and imaging of spectral signatures inside containers have considerable potential. However, realization of this potential is both mediated by, and complicated by, effects of scattering.
8. **Summary/Abstract:** The long-term aim of this project has been an integrated spectral and imaging methodology on which to base technology development. We focused in this project on scattering-mediated spectroscopy because practical solutions can rely neither on transmission nor specular reflection geometries. We sought to clarify what scattering mechanisms are important for THz sensing of explosive materials, and then to develop stand-off methods to identify and discriminate those materials based on spectroscopic methods mediated by scattering. We conducted a coordinated experimental and theoretical investigation by developing a versatile THz laboratory, based on state-of-the-art electro-optical (EO) polymer sources and detectors.
9. **Technical Contents and Accomplishments**

9.1. DURIP-Assisted Terahertz Facility Construction

With additional funding from ONR DURIP Award N00014-06-1-0592, we constructed a THz experimental facility using sources and detectors based on electro-optical polymers, together with a femtosecond laser system. Our system achieved a wide- and continuous-bandwidth, without spectral notches or gaps, and supported a wide variety of experiments. This work was initially undertaken as an extension of an existing collaboration with Prof. Michael Hayden (Dept. of Physics, Univ. Maryland – Baltimore County). Our setup is shown schematically, and as realized on an optical table, in Figures 1 and 2, respectively.

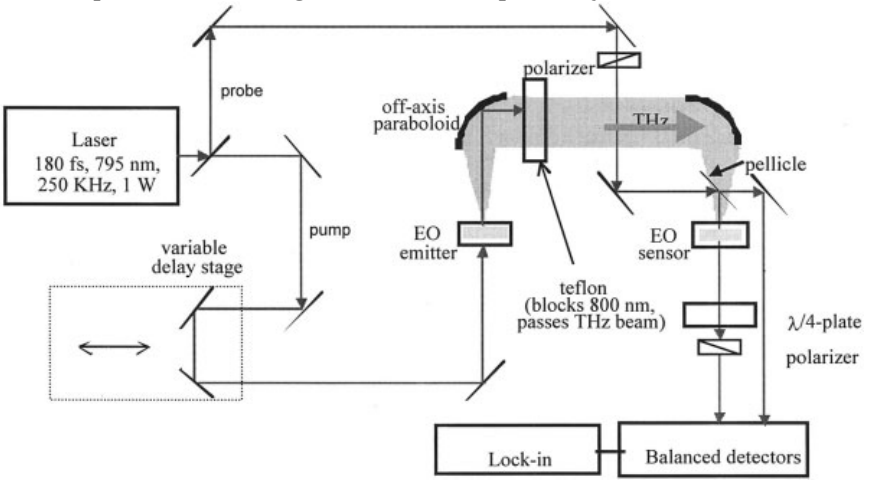

Figure 1. The femtosecond pump laser is incident on the EO polymer emitter, which generates a THz pulse via optical rectification. The THz pulse propagates to the EO polymer sensor, where it induces a change in the refractive index via the electro-optic effect. The polarization of the probe beam is modified by the changing refractive index in the sensor and detected via a crossed-polarizer arrangement and a balanced photodetector pair.

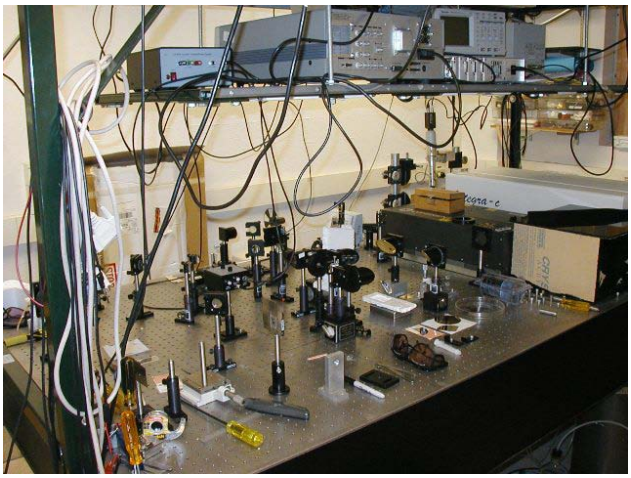

Figure 2. Physical realization of our THz time-domain spectrometer in the laboratory of co-investigator Antao Chen.

9.2. **Assessment of THz Scattering Mechanisms Pertinent to Explosive Materials**
At the outset of this project, fundamental questions were unresolved as to the importance of various scattering mechanisms in THz interaction with explosive materials. For example, the granular nature of plastic explosives suggested that volume scattering might be significant in determining spectral signatures of those materials, while the surface roughness of typically occurring masses of explosives suggested that surface reflection and scattering might dominate any volume effects.

We therefore first addressed volume scattering at THz frequencies using established multiple-scattering theory in granular polyethylene materials, which are commonly used in measurement of explosive spectral properties. THz absorption in polyethylene is small, so in pure polyethylene systems, volume scattering dominates the observed spectral attenuation. We explained the observed variation quantitatively (cf. Figure 3), in collaboration with Hayden's group at UMBC (Zurk et al., 2007).

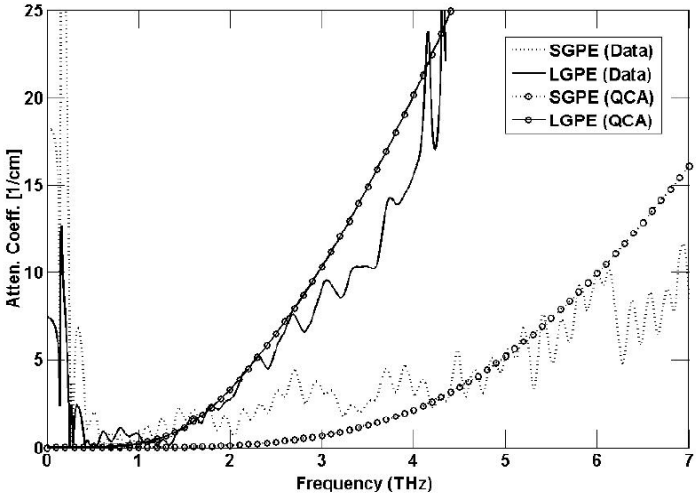

Figure 3. Spectral attenuation coefficients as observed and according to the Quasi-Crystalline Approximation (QCA) – with inputs determined by independent measurements of grain properties – for small-grain polyethylene (SGPE) and large-grain polyethylene (LGPE) (Zurk et al., 2007).

However, transmission observations of actual plastic explosives show that attenuation in those materials is far larger than in polyethylene and is dominated by absorption rather than scattering. Figure 4 (upper panel) shows the skin-depth (i.e., 1 e-folding length) for intensity in C-4, as a

function of wavelength, based on a simple model-fit to published data. THz penetration into C-4 and other plastic explosives is limited to distances generally well under 1 mm, which sharply limits any volume scattering effects relative to surface reflection and scattering. Moreover, the high attenuation of explosives implies that THz spectroscopic identification of such materials must be based not on transmission spectra, as seems to be assumed in some literature, but rather on spectroscopy using reflected or surface-scattered radiation.

The lower panel of Figure 4 shows, however, that the spectral surface reflectivity of C-4 does contain prospectively useful information, particularly near a 0.8 THz spectral feature characteristic of RDX, the primary component of C-4.

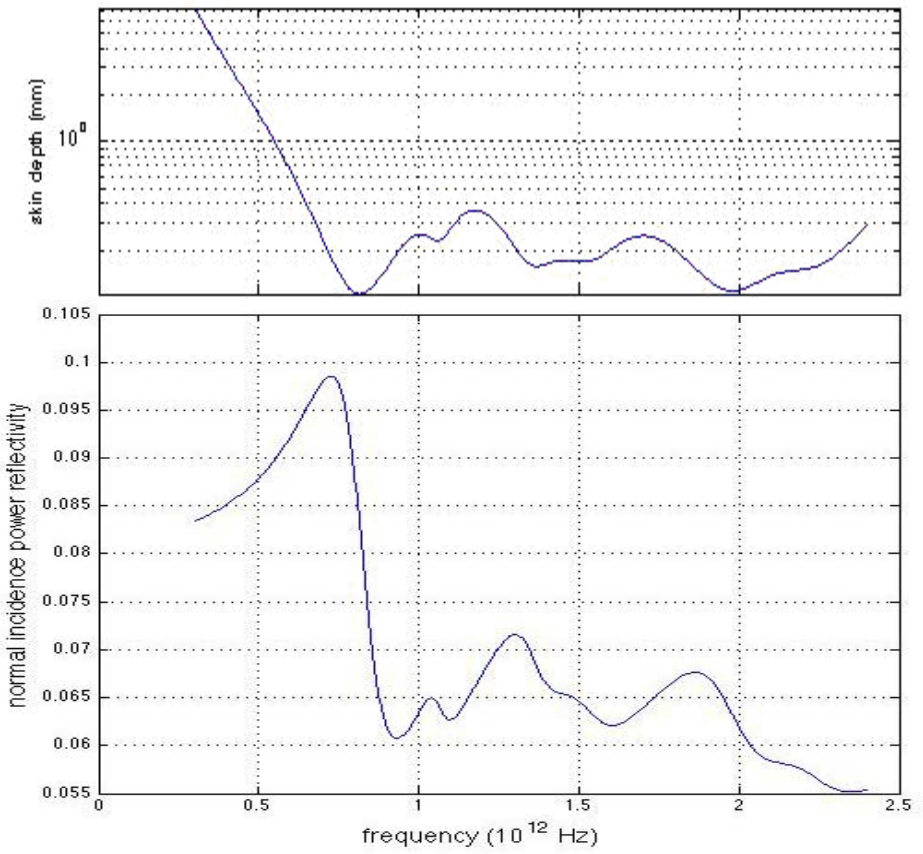

Figure 4. (upper panel) Skin-depth (e-folding length of power attenuation) in C-4, based on a simple model fit to published measurements. (lower panel) Calculated normal incidence power reflectivity of C-4 based on the same model fit and measurements.

9.3. **Importance of Incoherent Scattering**

Detection of explosives in practice will almost always require rapid scanning of uncooperative targets – i.e., targets that will not willingly present themselves to a sensor from specified angles or ranges. The observation of specularly reflected THz radiation for explosive detection (e.g., using a signature like that in Figure 4) is therefore impractical. Figure 5 illustrates the problem.

Robust detection methods must instead rely on THz radiation scattered incoherently from 100-micron-scale (i.e., THz-wavelength-scale) surface roughness on explosive charges. Such roughness will certainly occur on working explosive charges unless they are specially polished.

We therefore expect surface scattering to a reliable source of scattered signals which can, in principle, be observed over a wide range of target orientations of the target (which are unknown prior to detection). Our investigation has thus focused first on observing incoherently scattered THz radiation, and then on how spectral information can be recovered from such observations.

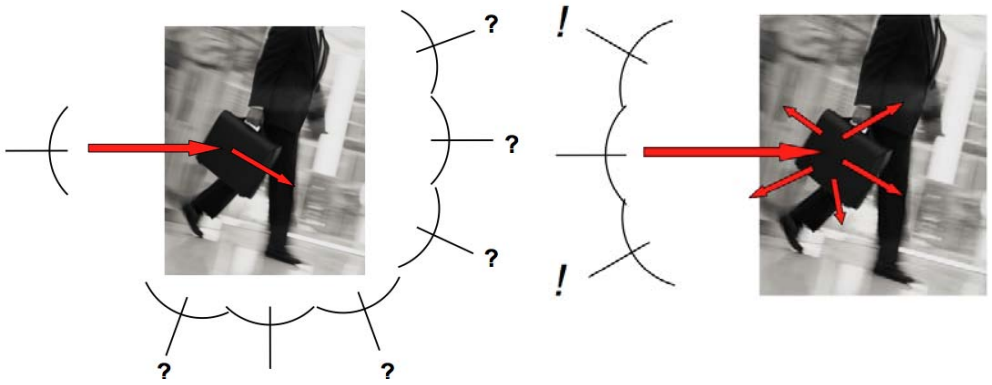

Figure 5. (left panel) Schematic representation of the problem of probing for explosive signatures using specularly reflected signals. The target orientation is unknown prior to detection (and the bearer of the target is unlikely to cooperate in presenting it favorably for detection), so detection of specularly reflected signals requires many sensors so as to view the target from many vantage points in the hope of spotting a specular reflection. (right panel) Incoherent scattering, by contrast, is diffuse in angle, and so can be observed reliably with just a few sensors, provided those sensors are sufficiently sensitive to detect the scattered radiation (which is considerably weaker than specularly reflected radiation).

9.4. **Observation of Incoherent Scattering**

Prior to work in this project, there had apparently (based on a literature search) been no systematic observation of incoherent scattered radiation at THz wavelengths. We have used THz time-domain spectrometry (THz-TDS) to obtain the first quantitative measurements of THz radiation scattered incoherently from rough surfaces.

Specifically, we used common sandpaper as a model rough surface (grit P80 in the data shown below) and coated it with a thin layer of gold to approximate a perfectly conducting rough surface. We measured roughness parameters of the coated sandpaper independently to inform theoretical modeling. We then used our THz time-domain spectrometer to measure scattered radiation in the specular direction for 30 separate patches on the rough surface, from which we computed the mean coherent power, individual incoherent scattered powers (power for a single realization minus the mean coherent power), and the mean incoherent scattered power, all as functions of THz frequency. A sample of results is shown in Figure 6. We also found the frequency dependence of coherent power to be in close agreement with simple theoretical modeling based on the Kirchhoff approximation.

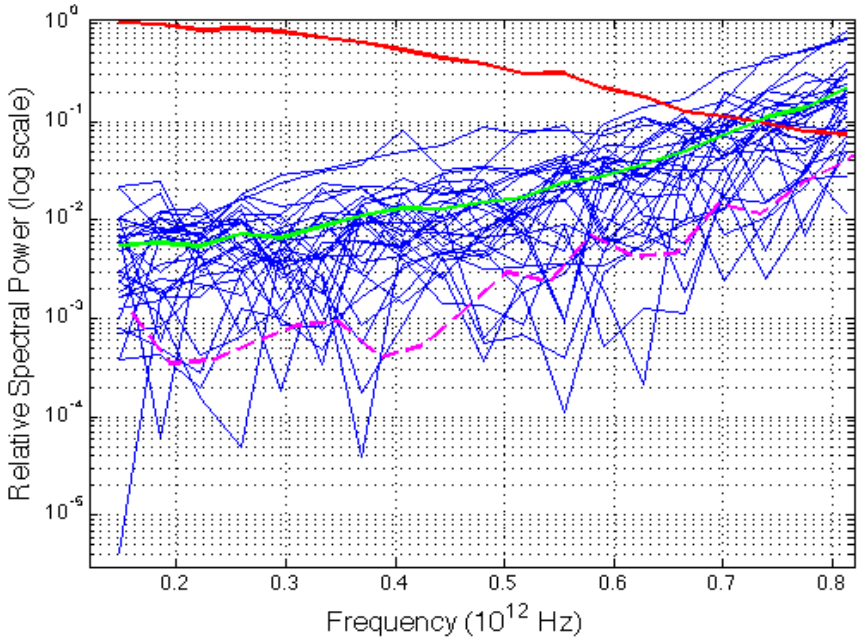

Figure 6. Coherent and incoherent scattered powers (relative to coherent power at 0.15 THz) as functions of THz frequency, from our THz-TDS experimental work on gold-coated P80-grit sandpaper. The red line shows coherent power derived from observations of 30 spatially distinct spots on the sandpaper. The coherent power decreases with increasing frequency in quantitative agreement with the prediction from Kirchhoff theory. The individual blue lines show individual realizations of the incoherent scattered power (measured power from one spot minus the coherent mean), and the green line shows the mean incoherent scattered power. At about 0.73 THz, the total scattered power becomes predominantly incoherent. The dotted magenta line shows an experimentally derived estimate of our THz-TDS system incoherence, which is in all cases about an order of magnitude less than the incoherent scattered power.

9.5. Spectral Information in Specular Incoherent Scattering Recovered Using a Wavelet Method

A perfectly conducting surface can show no spectral structure like that in the lower panel of Figure 4 because the conductor has no resonances to cause variations in its dielectric properties as a function of frequency. In order to investigate spectral information in rough surface scattering, we used roughened surfaces of alpha-lactose-monohydrate mixed (for binding purposes) with polyethylene. Alpha-lactose-monohydrate had a prominent spectral resonance at 0.53 THz which is qualitatively similar to the characteristic resonance of RDX at 0.8 THz; it thus constitutes a useful laboratory analog of RDX while avoiding the practical difficulties of dealing with significant quantities of that material.

We used sandpaper with several roughnesses to impress surface roughness on pellets of lactose and polyethylene, and measured specularly scattered radiation using THz-TDS on progressively rough surfaces starting from smooth and ranging up to the roughness associated with P80-grit sandpaper. Figure 7 shows the spectral response in specularly scattered intensity (differentiated as a function of frequency to show the location of the resonance more clearly). The spectral signature of the 0.53-THz lactose resonance is clearly apparent in data for smooth lactose, but rapidly degrades with increasing roughness, and becomes essentially invisible in the case of P80-grit roughness.

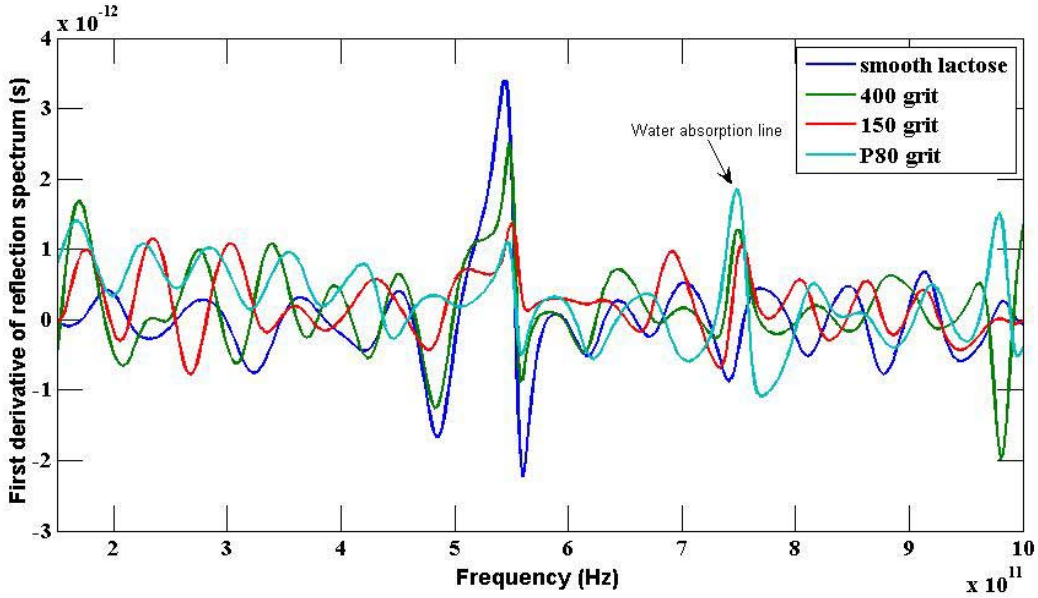

Figure 7. First derivative of normalized reflection spectral amplitude of lactose pellets of different roughness grits.

We have developed a method using wavelet decomposition of the frequency-domain signal, however, which successfully recovers the location of the resonance even in this latter case. The method works essentially by separating variations in the frequency-domain signal on the specific frequency scale of the resonance from other, extraneous variations caused by incoherent scattering, thus providing a statistically sound basis for detection of the resonance (Figure 8) even when it is obscured by incoherent scattering effects. Details are available in our 2010 SPIE paper (Arbab et al., 2010) and in a forthcoming paper for submission to *Optics Express*. We have worked with the University of Washington Center for Commercialization in filing a US patent application on our method.

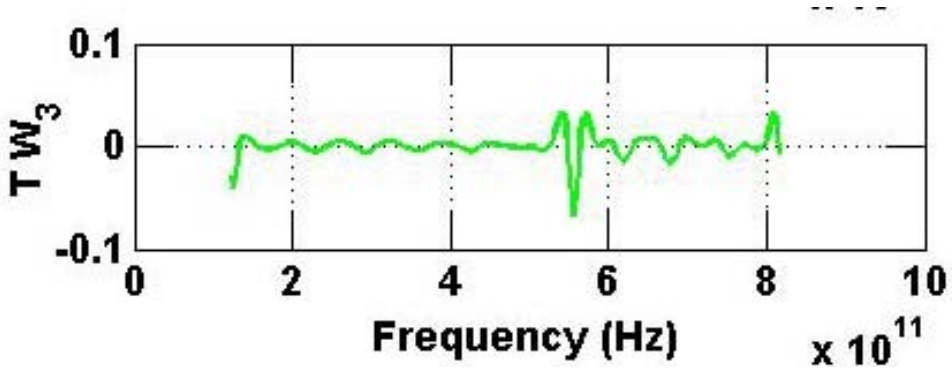

Figure 8. Coefficients of the Maximal Overlap Discrete Wavelet Transform on the scale in frequency closest to the scale of the 0.53-THz transition in Figure 7, derived from the P80-grit (differentiated) data in that figure. Whereas the variation associated with the lactose resonance is obscured by incoherent scattering in Figure 7, it appears clearly in this decomposition of the data – thus allowing detection of the material even in incoherently scattered data.

9.6. **Backscattering Spectroscopy**

Finally, for backscattering at angles far from vertical incidence, the scattering is due predominantly to roughness on scales that are small compared to the radiation wavelength (albeit modulated by larger-scale surface slopes). The theory for such scattering is well-developed and permits straightforward prediction of relative backscattered intensities as functions of frequency in the vicinity of a material resonance such as those shown in Figures 4 and 7. On this basis, we predict that the effect of characteristic material resonances in the THz region on backscattered power will also be useful for spectroscopic identification of materials. Figure 9 shows theoretical calculations for circularly polarized backscattering, which we predict to be particularly insensitive to the target aspect (and thus useful for detection of targets whose orientation is unknown a priori). We are working to publish this prediction with the aim of stimulating the (difficult) experimental work necessary to test it and lead toward its application in practical, robust THz explosive screening.

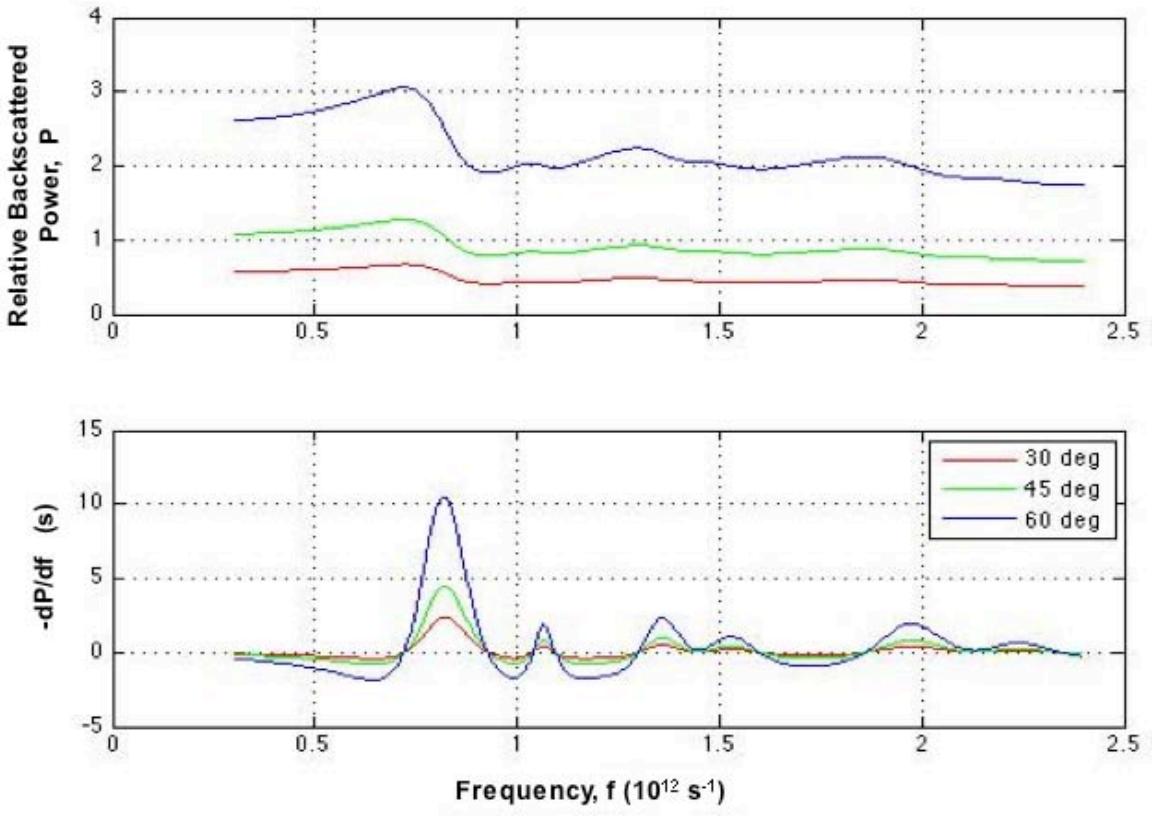

Figure 9. Theoretical predictions for spectroscopic variation of circularly polarized backscattered (incoherent, ensemble-averaged) intensity for a rough surface on C-4. The three colored lines represent predictions at 3 incident angles. All clearly show the dominant RDX resonance at 0.8 THz, along with effects of more minor resonances at higher frequencies. The lower panel shows the negative of the derivative with respect to frequency of the computed curves in the upper panel. It is essential that the position in frequency of the resonance signatures does not vary with incidence angle (here indicated as the angle from normal incidence) – thus material resonances in targets with unknown orientation appear at predictable frequencies and detection can be achieved without special orientation of the target.

10. **Deliverables, Personnel, Awards, Publications, Presentations, and Patents**

Deliverable	Date
"Retrieval of terahertz spectroscopic information in the presence of the rough surface scattering effects," M. H. Arbab, D. P. Winebrenner, Antao Chen, and E. I. Thorsos, US Provisional Patent Application 61/435,871, January 25, 2011, filed by University of Washington Center for Commercialization.	January 25, 2011
Final Technical Report (this report) with SF298	January 2011

Table 1. Deliverables

	Total #	Name	Organization
PIs	2	Dale Winebrenner	**University of Washington**
		Lisa Zurk	**Portland State University**
Co-PIs	2	Antao Chen	**University of Washington**
		Eric Thorsos	**University of Washington**
Graduate Students / Research Assistants	3	M. Hassan Arbab	**University of Washington**
		Scott Schecklman	**Portland State University**
		Sam Henry	**Portland State University**
Post Docs	1	Zhen Zhou	**University of Washington**

Table 2. Personnel Information

	Name	Award (Year Received)	Prize (Year Received)	Recognition (Year Received)
PIs	Lisa M. Zurk	ONR Faculty Award (2005)		
	Lisa M. Zurk	NSF CAREER Award (2006)		
	Lisa M. Zurk	Presidential Early Career Award for Scientists and Engineers (2006)		
Co-PIs	Antao Chen	Applied Physics Laboratory Science and Engineering Award (2006)		

Table 3. Awards/Prizes/Recognitions

Final Report for ONR CODE 30 CIED 6.1 Basic Research Effort

Name	Publication (Date)	Conference Presentation (Date)	Patent (Date)
L. Zurk, B. Jouni, F. Farahbakhshian, D. P. Winebrenner, E. I. Thorsos, A. Chen, M. R. Leahy-Hoppa, L. M. Hayden		"Scattering calculations for evaluation of terahertz detection of explosive material," presented at the 7th International Symposium on Technology and Mine Problem, Monterey, CA (May 2-5, 2006).	
Z. Zhou, A. Chen, J. Zhang, L. M. Zurk, B. Orlowski, E. I. Thorsos, D. P. Winebrenner, and L. R. Dalton	"Impacts of terahertz scattering on the reflection spectrum for explosive detection," *Proc. SPIE*, vol. 6772, pp. 67720T:1-7 (2007).		
L. Zurk, B. Orlowski, G. Sundberg, D. P. Winebrenner, E. I. Thorsos, and A. Chen	"Electromagnetic scattering calculations for terahertz sensing," *Proceedings of SPIE*, vol. 6472, pp. 64720A:1-9 (2007).		
L. M. Zurk, B. Orlowski, G. Sundberg, Z. Zhou, and A. Chen		"Terahertz scattering from a rough granular surface," IEEE Antennas and Propagation Society International Symposium, AP-S, pp. 4929-4932 (2007).	
L. M. Zurk, B. Orlowski, D. P. Winebrenner, E. I. Thorsos, M. R. Leahy-Hoppa, and L. M. Hayden	"Terahertz scattering from granular material," *J. Opt. Soc. Am. B*, vol. 24, No. 9, pp. 2238-2243 (2007).		
S. Schecklman, G. Sundberg, L. M. Zurk, A. Chen, and M. H. Arbab		"THz scattering from random rough surfaces," Progress In Electromagnetics Research Symposium (PIERS), Cambridge, MA (July 2-6, 2008).	

M. H. Arbab, D. P. Winebrenner, A. Chen, D. Wang, E. I. Thorsos, and L. M. Zurk		"Measurement and application of incoherent terahertz scattering using time-domain spectroscopy," 33rd International Conference on *Infrared, Millimeter and Terahertz Waves* (2008).	
M. H. Arbab, A. Chen, E. I. Thorsos, and D. P. Winebrenner	"Effect of surface scattering on terahertz time domain spectroscopy of chemicals," *Proc. SPIE*, vol. 6893, pp. 68930C:1-8 (2008).		
L. M. Zurk, G. Sundberg, S. Schecklman, Z. Zhou, A. Chen, and E. I. Thorsos	"Scattering effects in terahertz reflection spectroscopy," *Proc. SPIE*, vol. 6949, pp. 694907:1-8 (2008).		
S. C. Henry, L. M. Zurk, and R. Campbell	"Measurement and modeling of dielectric tube waveguides for terahertz pulses," *Proc. of SPIE*, vol. 7215, pp. 72150N:1-9 (2009).		
M. H. Arbab, D. P. Winebrenner, E. I. Thorsos, and A. Chen	"Application of wavelet transforms in terahertz spectroscopy of rough surface targets," *Proc. SPIE*, vol. 7601, pp. 760106:1-7 (2010).		
M. H. Arbab, D. P. Winebrenner, E. I. Thorsos, and A. Chen	"Retrieval of terahertz spectroscopic signatures in the presence of rough surface scattering using wavelet methods," Appl. Phys. Lett., vol 97, 181903 (2010).		
D. P. Winebrenner, M. H. Arbab, A. Chen, and E. I. Thorsos.			See Table 1

Table 4. Publications, Conference Presentations and Patents

11. **References:** (In support of Sections 7-9 above.)

L. M. Zurk, B. Orlowski, D. P. Winebrenner, E. I. Thorsos, M. R. Leahy-Hoppa, and L. M. Hayden, "Terahertz scattering from granular material," *J. Opt. Soc. Am. B*, vol. 24, No. 9, pp. 2238-2243, Sept. 2007.

M. H. Arbab, D. P. Winebrenner, E. I. Thorsos, and A. Chen, "Application of wavelet transforms in terahertz spectroscopy of rough surface targets," *Proc. SPIE*, vol. 7601, pp. 760106:1-7 (2010).

REPORT DOCUMENTATION PAGE

Form Approved
OMB No. 0704-0188

PLEASE DO NOT RETURN YOUR FORM TO THE ABOVE ADDRESS.

1. REPORT DATE *(DD-MM-YYYY)*	2. REPORT TYPE	3. DATES COVERED *(From - To)*
31-01-2011	Final	Aug 05 - Dec 09

4. TITLE AND SUBTITLE

"Final Report: Basic Research at the University of Washington to Counter Improvised Explosive Devices"

5a. CONTRACT NUMBER

5b. GRANT NUMBER

N00014-05-1-0843

5c. PROGRAM ELEMENT NUMBER

6. AUTHOR(S)

Jeffrey A. Simmen, Eric I. Thorsos, William E. Asher, Antao Chen, Lawrence A. Crum, William T. Elam, Maya Gupta, Yasuo Kuga, Caren Marzban, and Dale P. Winebrenner.

5d. PROJECT NUMBER

5e. TASK NUMBER

5f. WORK UNIT NUMBER

7. PERFORMING ORGANIZATION NAME(S) AND ADDRESS(ES)

Applied Physics Laboratory, University of Washington
1013 NE 40th St.
Seattle, WA 98105

8. PERFORMING ORGANIZATION REPORT NUMBER

9. SPONSORING/MONITORING AGENCY NAME(S) AND ADDRESS(ES)

Office of Naval Reserarch
875 N. Randolph Street
Arlington, VA 22203

10. SPONSOR/MONITOR'S ACRONYM(S)

ONR

11. SPONSOR/MONITOR'S REPORT NUMBER(S)

12. DISTRIBUTION/AVAILABILITY STATEMENT

Distribution Statement A: Approved for Public release, distribution unlimited

13. SUPPLEMENTARY NOTES

14. ABSTRACT

This final report describes research on developing new technologies and approaches for countering Improvised Explosive Devices (IEDs). The work comprised eight projects, including two prediction projects, one that developed methods for identifying explosive materials using x-ray emission spectra, and another that developed similarity based learning architectures to improve pattern recognition for real time decision-making. One of five detection projects researched a nonlinear spectroscopic technique of sum frequency generation as a novel remote sensing system for detecting trace amounts of explosive chemicals on surfaces. Another project explored the idea that explosive chemicals change the ionic field surrounding an explosive in detectable ways, in particular, the idea that the ionic field can be probed using electro-optic polymers in the form of micro-ring resonators attached to long optical fibers to potentially provide standoff detection capability. The detection projects also included a comprehensive study of ultra-wideband imaging using distributed sources and receivers over a wide range of electromagnetic frequencies. Another developed fundamental theory and methodology for rapid and reliable detection of change points in multivariate data streams; this research can contribute to improvements in real time decision making when multiple sensors yield multiple streams of data. The final detection project was an investigation to understand the scattering properties of concealing structures and target materials for electromagnetic radiation at terahertz frequencies. The only mitigation project contributed to the long term goal of developing an in-field capability for stopping uncontrolled bleeding from major blood vessels caused by explosions.

15. SUBJECT TERMS

chemical detection with nonlinear optical methods, chemical detection with fiber optic sensors, controlling bleeding with focused ultrasound, chemical detection using X-ray spectroscopy, similarity measures for data analysis, object detection with wide band electromagnetic waves, change detection with multiple data streams, and chemical detection with terahertz radiation.

16. SECURITY CLASSIFICATION OF:			17. LIMITATION OF ABSTRACT	18. NUMBER OF PAGES	19a. NAME OF RESPONSIBLE PERSON
a. REPORT	b. ABSTRACT	c. THIS PAGE			Jeffrey A. Simmen
U	U	U	U	88	19b. TELEPHONE NUMBER *(Include area code)* 206-543-1300

Reset

Standard Form 298 (Rev. 8/98)
Prescribed by ANSI Std. Z39.18